UNIVERSITY
OF GÄVLE

FACULTY OF ENGINEERING AND SUSTAINABLE DEVELOPMENT
Department of Industrial Development, IT and Land Management

Design of a carbon fibre rim for a fuel efficient competition vehicle

Pau Gomà Golanó

2014

Thesis for Bachelor of Science in Mechanical Engineering

Supervisor: Per Blomqvist
Examiner: Kourosh Tatar

Acknowledgements

This report is the result of my bachelor thesis that was carried out in the University of Gävle, in Sweden, during the spring 2014.

I would like to thank the people of the HiGtech Team who helped me in any way, especially Mattias Oppitz and Jonas Söderström.

I would like to extend my appreciations to my supervisor, Per Blomqvist and my examiner Kourosh Tatar, for their guidance during the thesis.

Finally, I would also like to thank my family and especially my parents.

Pau Gomà Golanó

Abstract

Motivated by the persistently pursued weight reductions in a vehicle projected for a fuel efficiency competition, this thesis deals with designing new and lighter rims for the vehicle. The aim of the thesis is to design the rims with a carbon-fibre reinforced polymer, a lightweight composite material. A profound study on this kind of material is also presented, since it could be useful for lighten, subsequently, other parts of the vehicle. The thesis is based on a review of literature to acquire a theoretical framework. The design process and its validation is supported by finite element analyses.

The preliminary design starts with a closed V profile, which appears to be a viable and adequate option for the application. The rim is divided into three parts, the contour and two sidewalls. By modelling and simulating the rim, the profile of each part is optimized and information about the stress´s state is acquired. Therefore the layered structure for the different parts are defined by taking the optimum proportions of the fibre's orientations into account. The parts are then simulated making use of a layered element which in the end validates the design.

The reserve factors found are 1,67 for the contour and around 1,5 for the sidewalls, which indicates the good adjustment of the design between safety and performance. On the other hand, an estimation for the weight reduction is calculated, which achieves values around 17% on the better cases. With further work on the manufacturing process the design can in the end offer a reasonable saving of weight.

Table of Contents

List of figures

List of tables

1 Introduction

This introduction offers a brief contextualization on the topic as well as the aims and limitations of the present thesis. The disposition of the thesis is also explained.

1.1 Background

With the world involved in an advancing global warming, we have started to be concerned about the environment and how we could take care of it since just few decades ago. Nowadays the strategy has changed into reduce consumptions and pollution. The governments and institutions are now setting aims of decrease the emissions during the next decades (the EU has committed to cutting its emissions to 20% below 1990 levels [1]). Accordingly, lately the research and industry faces with reduce consumptions and develop new and green energy sources.

The automotive sector has been dragged to innovate in this way as well, in order to reduce emissions and increase the fuel efficiency (road transport alone contributes about one-fifth of the EU's total emissions of carbon dioxide (CO_2) [2]). This is done by improving old technologies and developing new ones. One of these growing new technologies is in the field of materials engineering. Coming from aerospace and aeronautic industries, now the composite materials are being introduced to the automotive sector.

Composite materials have the potential of reducing the vehicle weight substantially while maintaining great mechanical properties and this, of course, has a direct effect on fuel consumption. One of the remarkable composite materials with a large future in this sector is the group of carbon fibre reinforced polymers (CFRP), [3] and [4].

1.2 Purpose

The purpose of this thesis is to develop a rim for an efficiency competition vehicle. More specifically, it will be for the vehicle from the team of the Gävle University College (Swedish: Högskolan i Gävle) called HiGtech team which participates in the Shell Eco-marathon®. In this competition, participants design and build their vehicles to achieve the highest possible fuel efficiency.

One of the things that the HiGtech team wants to do, to further improve the vehicle, is to reduce the weight of the current rims. The current aluminium rims are bicycle rims adapted, therefore they thought about building these ones with a lighter material as could be a composite material. This, then, is the purpose of the present thesis.

1.3 Aims

The aim of the thesis is to develop a rim made of carbon fibre reinforced polymer (CFRP). The rim has to withstand safely the stresses imposed by the characteristics and operating conditions of the HiGtech team's vehicle, and also be as light as possible.

The thesis also seeks to give an overview of the carbon fibre reinforced polymers, presenting its traits and properties to finally size the laminate for the rim.

The design aims match with the parts already selected or designed by the HiGtech team.

1.4 Boundaries

The thesis has aims to complete but also frontiers so that the purposes will not be lost. These ones are:

The tire for the wheel is already selected so it will be out of the study. The shaft that connects the wheel with the vehicle's body is already dimensioned and it is one of the limits of the design as well as the break system. Any business plan for commercialization is also out of this thesis.

1.5 Disposition of thesis

The thesis starts explaining the methods used throughout the work in chapter 2. Followed for an overview to all the theories involved somehow on the thesis in chapter 3. The next one, chapter 4, shows the calculations needed before starting the design chapter. Chapter 5, *Design of the rim*, exposes the results and explains the design process followed during the work. The last chapter is the discussion and conclusions of the thesis.

2 Methods and procedure

This chapter explains the methods used and describes the procedure followed during the work. The development of the thesis followed approximately the disposition of this report.

First a literature review was done in order to acquire and consolidate the necessary knowledge. The literature review was focussed in three main topics, the ones considered very important for the right development of the thesis. First the continuum mechanics was reviewed; this was focused on the deformable solid mechanics, since it describes the elastic behaviour of the rim under loads. It was done by taking the non-isotropic properties of composite materials into account. The sources consulted for the continuum mechanics theories were [5], [6], and [7]. Then composite materials were studied deeply, focussing in carbon fibre reinforced polymers, since the material was a crucial factor in the design. The general characteristics, mechanical properties and failure modes were reviewed. The sources consulted for the composite materials part were [8], [9], [10] and [11]. Also the finite element method and finite element analysis were somewhat reviewed in order to understand better how works the software used during the thesis development as well as for working properly with it.

The next step was to understand correctly the functions and requirements that the design had to accomplish. This part took care of the joints between the rim and the already designed or selected parts on the vehicle and also of the competition's rules. Furthermore the loads that the rim had to withstand were calculated using the classic physic and mechanic laws.

Following, the design process started selecting a basic preliminary design. This was done looking into some related literature and research ([12] and [13]). The design was then optimized using statistical methods [14]. For doing that some variables, dimensions which change rim's geometry, were selected. Then the procedure was to simulate models or samples with different combinations of these variables' values. For the simulations the package software ANSYS® 15.0 was used. The responses observed were the stresses in determinate points of the rim. Then different response surfaces ([14] and [15]) were drawn with the purpose of visualise the effect that each variable had into the response (the stresses). The final shape of the rim was defined; using for that the variables' values that achieved the lowest stresses. With the geometry defined, simulations with different load cases were carried out for finding the stresses and its orientations, essential information for afterwards sizing the laminate.

Subsequently the laminate configuration for each part of the rim was defined. This process started with analysing the stresses found before and looking for the optimum distribution of the layers that compound the laminate. This was done with the help of some tables, presented on [16], which provide favorable configurations of the laminate given the stress distribution. Then the whole assembly was studied and the joints between the parts were defined.

Finally, in order to validate the design, the rim was modelled using ANSYS® ACP 15.0 (ANSYS Composite PrepPost) which allows the definition, simulation and post-processing with layered materials, as is the case of composite materials. The deformations under the design loads and the reserve factors for the failure criterion were checked. At the end a brief search in order to find a possible manufacturing process was done.

3 Theoretical framework

3.1 Continuum mechanics notions: deformable solids mechanics

3.1.1 Introduction

Continuum mechanics is a branch of mechanics that study the deformation of a medium made out of matter subjected to forces. It is typically divided between solid and liquids but the starting theories are the same. This section wants to review briefly the main theories of continuum mechanics involved on the thesis, focussing on the solid continuum mechanics.

The fundamental hypothesis for the continuum mechanics, as the name indicates, is that the matter of a medium is considered continuously distributed and also the variables involved on the problem have to be continuum (mass distribution, velocity, pressure, etc.).

In a microscopic scale, the continuum mechanics treats the medium as a great network of particles that interact between each other. It studies the variation of the cohesive forces between particles from a reference state, not its absolute values. The classical simile is that two particles are connected by a spring. To relating the forces acting between both particles and the variation of the spring's length, a characteristic property of the spring is used, *k*. Then for the Figure 1 below, one can relate the physical phenomenon with

$$\Delta f = k\,\Delta a \quad ,$$

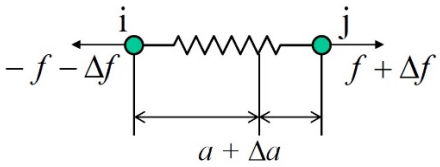

Figure 1. Spring's simile for the cohesive forces between two particles, i and j. [7].

where *f* is the first force acting at each particle and *a* is the original spring's length. Then with an increment on the forces Δf there is also a proportional increment on the length Δa, with the proportionality constant *k*.

Macroscopically, one studies the deformation that occurs on the matter due to the stresses or vice versa. The principal relationship between both is the Hooke's law; which comes from the same principles looked at the microscopic view. Figure 2 represents the one-dimensional elastic problem where one can define the tensile stress σ as:

$$\sigma = \frac{dF}{dA} \quad ,$$

and the strain ε, or elongation, as

$$\varepsilon = \frac{du}{dL} \quad .$$

Then the Hooke's law is defined as

$$\sigma = E\varepsilon \quad ,$$

where *E* is the modulus of elasticity, an elastic characteristic of each material. It is

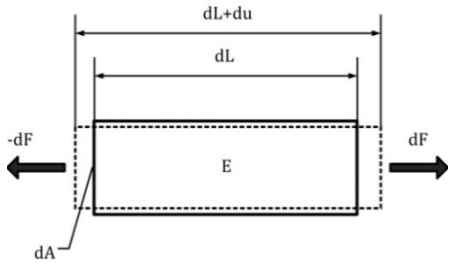

Figure 2. One-dimensional elastic problem's schematic. The deformations (du) are related by the elastic properties (E) with the stresses (dF/dA).

the relation between the stress that is applied to the solid and the consequent strain that it produce.

3.1.2 Stress

The introduction presented the one-dimension model that now can be extrapolated to a three-dimensional one.

The stress vector defines the forces between the internal surfaces of the bodies subjected to loads. Considering an infinitesimal point *P* of one elastic body subjected to loads and a plane *S* touching this point with its normal vector $\vec{n}$, the stress vector $\overrightarrow{t_n}$ is defined as:

$$\overrightarrow{t_n} = \sigma\, \vec{n} \quad ,$$

where σ was defined previously as the force Δf acting on an small area ΔA. Figure 3 represents this definition.

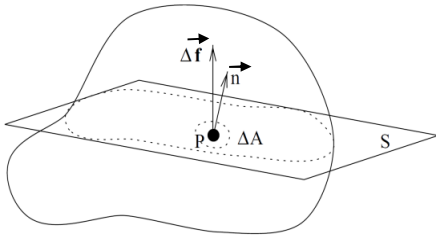

Figure 3. Definition of the stress vector [17]. At each point P, touched for a plane S with its normal vector $\vec{n}$, a stress vector is acting defined for the force and the small area on the point.

Then one wants to define all the stress state in this point *P*. Since there are infinite planes *S* as well as infinite tension's vectors, it is necessary to use a tensorial magnitude to represent this state. In a Cartesian coordinate system, the stress tensor is:

$$[\sigma] = \begin{bmatrix} \sigma_{xx} & \sigma_{yx} & \sigma_{zx} \\ \sigma_{xy} & \sigma_{yy} & \sigma_{zy} \\ \sigma_{xz} & \sigma_{yz} & \sigma_{zz} \end{bmatrix}_{x,y,z} \quad ,$$

and the representation of its components is shown on Figure 4. The stress vector is decomposed then in three components. On one hand the normal stress (σ_{ii}), which acts perpendicularly to the plane. It is placed on the main diagonal of the tensor. On the other hand the two shear stresses (σ_{ij}), the components that are acting tangentially to the plane.

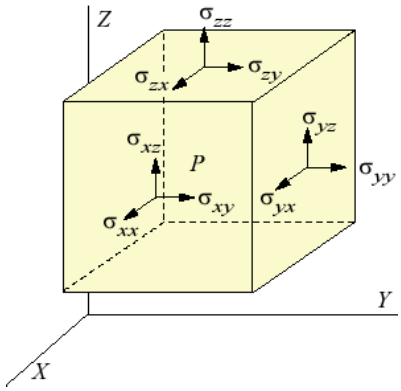

Figure 4. Three-dimensional stress state on a point P, defined using the Cartesian coordinate system. All components are in positive sense. [18].

The stress tensor is a symmetric matrix since there exists reciprocity between the shear stresses for accomplish equilibrium of moments ($\sigma_{ij} = \sigma_{ji}$) [5].

Although this representation is enough to define the stress state (since it is done with a three independent vector basis), this is only the representation of the stresses on three planes. If we think about one small point of the body there is one stress vector for each direction on the space. The Figure 5 illustrates this phenomenon in a two-dimensional form; the representation of all the stress vectors at each point draws an ellipsoid called ellipsoid of Lamé (in red) [5]. There are three particular stresses that maintain perpendicular at their planes (or collinear to the plane normal vector). Those are the principal stresses, and on the planes they are acting there are not shear stresses since the stress is only normal. The figure shows in purple two of

the three principal stresses acting on a point *p*. The normal vectors of the planes they are acting (n_1 and n_2) are aligned with the ellipsoid axes.

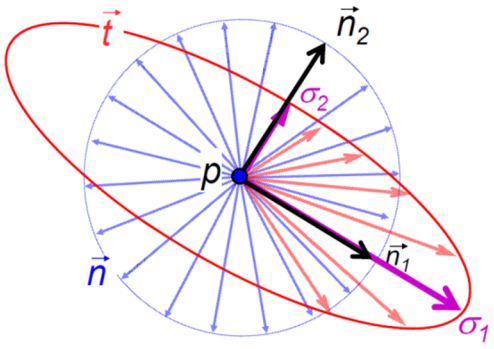

Figure 5. Two-dimensional representation of: in red, the ellipsoid of Lamé; in blue, normal vectors at one point p; in purple, two principal stresses and in black the normal vectors of the planes where the principal stresses are acting. [7].

In a mathematical way, the principal stresses σ_1, σ_2, σ_3 are the eigenvalues of the stress tensor and the eigenvectors are the principal directions. They are the invariants of the matrix and physically they are the stresses that maintain perpendicularly to their planes. Then changing the coordinate system the stress tensor can be expressed as:

$$[\sigma] = \begin{bmatrix} \sigma_1 & 0 & 0 \\ 0 & \sigma_2 & 0 \\ 0 & 0 & \sigma_3 \end{bmatrix}_{1,2,3} ,$$

usually defined in the order: $\sigma_1 > \sigma_2 > \sigma_3$,

where the tensile stresses are positive and compressive are negative. They are called first, second, and third principal stresses. The first principal stress then is the highest value of the normal stress acting at some plane of each point of the body and the third one is the lowest (in absolute values).

These stresses will be very useful during this thesis to find possible failure points and to orientate the fibres of the composite material. Afterwards it will be presented a tool to represent the stress state of one point in order to identify the principal stresses.

3.1.3 Strain

The strains can be studied in the same way as the stresses. Defining a tensor all the strain state becomes defined at one point. Using the Cartesian coordinate system the tensor is:

$$[\varepsilon] = \begin{bmatrix} \varepsilon_{xx} & \varepsilon_{yx} & \varepsilon_{zx} \\ \varepsilon_{xy} & \varepsilon_{yy} & \varepsilon_{zy} \\ \varepsilon_{xz} & \varepsilon_{yz} & \varepsilon_{zz} \end{bmatrix}_{x,y,z} .$$

One the main diagonal the strains terms describes longitudinal elongations in the different axes, and the other terms represent angular distortions between the axes. Then it is also possible to find directions where the elongations are only longitudinal and normal to their planes. They are the principal strains, the eigenvalues of the strain tensor:

$$[\varepsilon] = \begin{bmatrix} \varepsilon_1 & 0 & 0 \\ 0 & \varepsilon_2 & 0 \\ 0 & 0 & \varepsilon_3 \end{bmatrix}_{1,2,3} ,$$

and they are also sorted as: $\varepsilon_1 > \varepsilon_2 > \varepsilon_3$.

In isotropic materials the axes of the stress and strain ellipsoids are coincident. Then the principal strains directions coincide with the principal stresses ones. For another types of materials, as composite materials, this does not happen[1].

3.1.4 Generalized Hooke´s law

With the stresses and strains defined it is possible to present the generalized Hooke´s law:

$$\{\bar{\varepsilon}\} = [C]\{\bar{\sigma}\} \quad ,$$

where the constitutive matrix [C] contains the constants of the material. These are the modulus of elasticity *E*, the shear modulus of elasticity *G* and the Poisson's ratio υ. On an isotropic material, where the properties are equal at any orientation, many of these constants on the matrix [C] become zero since there is symmetry at many planes.

Giving an overview of the elastic properties, the modulus of elasticity *E* is the relation between normal stresses and longitudinal strains (change of volume); the shear modulus *G*, is the relation between shear stresses and angular distortions (change of shape); and finally the Poisson's ratio υ, which is the ratio of transverse contraction strain to longitudinal extension strain in the direction of the tensile stresses.

In the particular case of study, carbon fibre reinforced polymers are treated as an orthotropic material [2] therefore from now on this kind of materials will be mentioned and presented. In the appendix A, the generalized Hooke´s law for isotropic and orthotropic materials is presented in more detail.

3.1.5 Plane stress

When the stress state is mainly acting only in one plane, it is simplified as a plane stress. It means that the stress study becomes two-dimensional.

In this thesis the elements studied are usually thin plates and the stress state will therefore be usually estimated as plane stresses. The general elasticity model in a plane stress for isotropic and orthotropic materials is exposed below. Figure 6 illustrates the plane stress state and define the elastic variables on it.

Now forward in the present work the shear stresses are denoted as τ_{ij} and the engineering shear strain is defined as $\gamma_{ij} = \varepsilon_{ij} + \varepsilon_{ji}$, since the notation used before is the mathematical one.

[1] See 3.2.5 *Isotropy and anisotropy*

[2] An orthotropic material is a particular case of an anisotropic material characterised for having at least two orthogonal planes of symmetry. The properties along the axis of these planes are considered equal. Such materials require nine independent variables (i.e. elastic constants) in their constitutive matrices while anisotropic materials do not have symmetry planes and need 21 independent variables.

- Isotropic materials:

An isotropic material does not present difference (theoretically) between any directions. The stress-strain relation in matrix form is:

$$\begin{Bmatrix} \varepsilon_x \\ \varepsilon_y \\ \gamma_{xy} \end{Bmatrix} = \begin{bmatrix} \frac{1}{E} & \frac{-\upsilon}{E} & 0 \\ \frac{-\upsilon}{E} & \frac{1}{E} & 0 \\ 0 & 0 & \frac{1}{G} \end{bmatrix} \begin{Bmatrix} \sigma_x \\ \sigma_y \\ \tau_{xy} \end{Bmatrix} \quad .$$

Note that there are only two independent elastic constants since exists a relation among them:

$$G = \frac{E}{2(1+\upsilon)} \quad .$$

- Orthotropic materials:

In an orthotropic material the elastic properties depends on the orientation where they are tested. The Hooke's law for these materials on plane stress state is:

$$\begin{Bmatrix} \varepsilon_x \\ \varepsilon_y \\ \gamma_{xy} \end{Bmatrix} = \begin{bmatrix} \frac{1}{E_x} & \frac{-\upsilon_{yx}}{E_y} & 0 \\ \frac{-\upsilon_{xy}}{E_x} & \frac{1}{E_y} & 0 \\ 0 & 0 & \frac{1}{G_{xy}} \end{bmatrix} \begin{Bmatrix} \sigma_x \\ \sigma_y \\ \tau_{xy} \end{Bmatrix} \quad .$$

In this case there are four independent elastic constants since there is also one relation between them:

$$\upsilon_{xy} = \upsilon_{yx} \frac{E_x}{E_y} \quad .$$

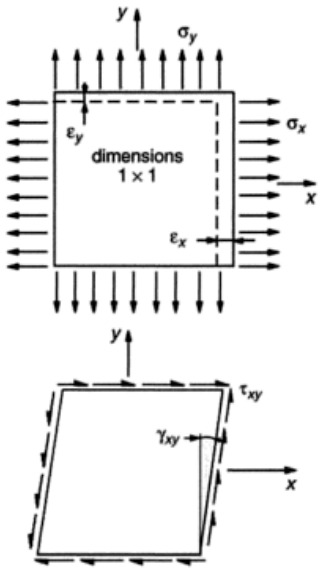

Figure 6. Plane stress's behaviour and the variables involved. [9].

3.1.6 Mohr's Circles

The Mohr's circles, named after Christian Otto Mohr, are the two-dimensional graphical representation of a tensorial magnitude [5]. In this section it will be briefly explained since it is a tool sometimes used during the thesis.

In continuum mechanics the Mohr's circle is used for the representation of the stress state (or strain) at a point of the body. The Figure 7 is the Mohr's circles representation of an arbitrary stress state. The abscissas represent the normal stress and the ordinates the shear stress of the stress components acting at one plane. Therefore, one stress vector t in red can be decomposed in the normal component (in blue) and the shear component (in yellow). The green area between the circles represents the tips of all the stress vectors acting at the point studied.

Each circle represents the stress state on the plane between the first and second principal stresses (red circle), between the second and third principal stresses (blue circle) and between the first and third principal stresses (green circle). The radiuses of these circles are the maximum shear stress located on the planes that the circles represent (τ_{12}, τ_{13}, τ_{23}).

In Mohr's circles it is also possible to identify the principal stresses (σ_1, σ_2 and σ_3). These ones are situated on the intersection between the three circles and the abscissas axis; following the definition of principal stress there is no shear stress its plane.

The angles on the Mohr's circles are the double that on the reality. For example the angle between the first and second principal stress is 180 degrees on the red circle but actually on the reality is 90 degrees. The maximum shear stresses are located between the principal stresses, and then the 90 degrees on the Mohr's circles are 45 in the reality.

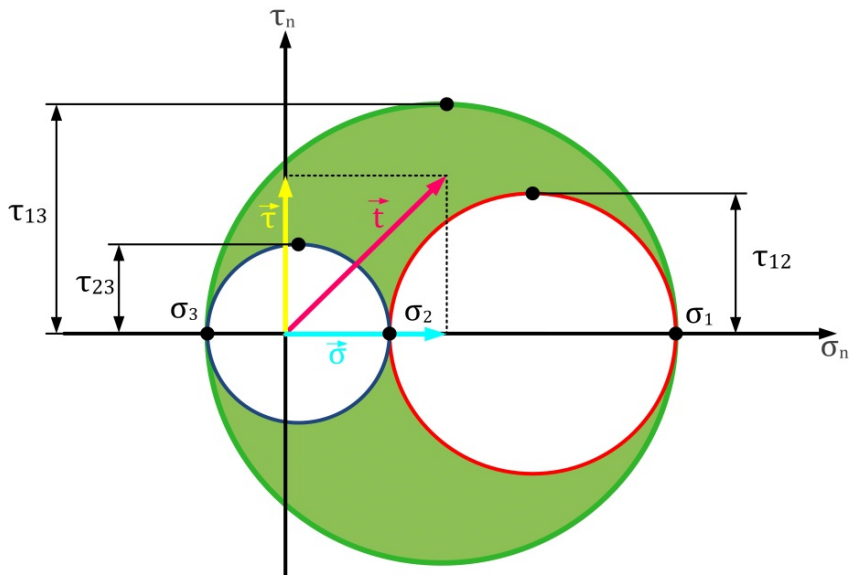

Figure 7. Mohr's circles for a three-dimensional stress state. In red an arbitrary stress vector, composed by: in blue the normal component and in yellow the shear component.

3.2 Composite materials

3.2.1 Introduction

A composite material is formed for two or more different materials or phases, the matrix and the reinforcements. The matrix is the weak part that contents the reinforcements and transmits the loads. The reinforcements are usually strong fibres which support the main part of the load.

The characteristics of a composite material depend on the combination of reinforcement and matrix. Different combinations of matrix and reinforcement derive on a material with more stiffness, or more strength, or more thermal resistance, etc. Therefore this versatility is an advantage that the composite materials have. Another great convenience is that they are usually lighter than the common engineering materials (like metals) while maintaining high mechanical properties [10]. So when working with composite materials, it is not only about design one product or piece, it is also about choose the right compound matrix–reinforcement to achieve the right material.

One of the more promising composite materials is the fibre reinforced polymer composite, widely used on the aerospace and aeronautic industries and it is starting to be important on automotive industry. In particular the carbon fibre reinforced polymer (CFRP) presents an excellent combination of low density, high modulus of elasticity, high fatigue resistance and thermal stability [4]. This thesis will therefore focus on the carbon fibre reinforced polymers (CFRP) since it is considered the optimum material for the application studied.

3.2.2 Matrix

In a composite material the matrix has many functions. First of all it holds the fibres together and protects those from the environment. It also distributes the loads evenly between the fibres and improves the transversal properties of the material. Moreover it improves impact and fracture resistance since sometimes the fibres are brittle.

There are three main groups of matrices with which the engineering composite materials can be divided. They are the metal matrix composites (MMC), ceramic matrix composite (CMC) and polymer matrix composites (PMC). In the present study only the polymer matrix composites will be mentioned as it was said on the point before.

Some of the most used polymers for matrices are polyimides, epoxies, polyesters and polycarbonates. Although epoxy resins are more expensive than other polymer matrices they have performance advantages over other ones. With better mechanical properties (modulus of elasticity, shear modulus, tensile strength) and with excellent adhesive properties (the ability to bond to the reinforcement), epoxy results the best option for high performance applications [8]. For this reason it was thought that an epoxy matrix would be the best option for rim's composite material.

Epoxy is a thermoset polymer [3] that is made by mixing two components, an epoxide resin and a hardener (or a curing agent). A curing process is necessary for achieve a solid and strong material. Curing is the process by which one of the reactants (epoxide and curing agent) are transformed from a low-molecular-weight material to a material with a highly molecular cross-linked network, forming covalent bonds between polymer chains [19]. This gives a high rigidity and dimensional stability to the material. Figure 8 below illustrates this process.

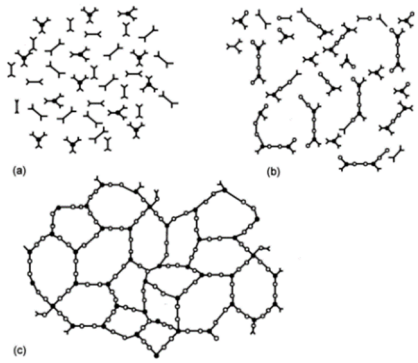

Figure 8. Curing of a thermoset. The process starts when mixing the components, still with monomer structure (a). Continues with branching between molecules, material becomes progressively gelled (b). It finishes as a fully cross-linked material, a cured thermoset (c). [20].

[3] A thermoset polymer is a material that is converted from a reactive fluid to a "set" or solid material through a called curing process.

Typical epoxy properties are presented on the Table 1. They are, however, generalizations for giving an order of magnitude. The reader should realize that given properties can vary significantly depending on the type, application and processing of the material.

Table 1. Properties of commonly used epoxy resins [8]. Contrasted with [10] and [21] .

Property	Symbol	Values	Units
Density	ρ	1.200	kg/m^3
Modulus of elasticity	E	4.500	MPa
Shear modulus	G	1.600	MPa
Poisson ration	ν	0,4	-
Tensile strength	$\sigma_{rupt.}$	130	MPa
Useful Temperature limit	T_{max}	90 to 200	ºC
Coefficient of Thermal Expansion	α	$11x10^{-5}$	ºC
Elongation	ε	2 (100ºC)	%
		6 (200ºC)	%
Temperature for curing	T_{curing}	100 to 150	ºC
Time for curing	t_{curing}	60 to 180	min

3.2.3 Reinforcements

Reinforcements have the role of increase the mechanical properties of the material. They can be presented in different forms as particles, flakes, whiskers, short fibres, continuous fibres, or sheets.

For polymer matrix composites, there are four main kinds of reinforcements used. These ones are glass fibres, carbon fibres, aramid fibres and boron fibres. The present thesis will focus at carbon fibre reinforced polymers (CFRP). The carbon fibres presents a really good mechanical properties (better than glass or aramid fibres), but also an acceptable price (much lower than boron fibres) [8]. Then they are considered more appropriate for the application studied, therefore other kinds of reinforcements will not be taken into account. Carbon fibres are usually presented as continuous fibres.

The carbon fibre can be found in two main types, with high modulus of elasticity (HM) or with high strength (HR). The difference of properties is due to its different routes of production. Carbon fibres are usually continuous, with a diameter around 7 μm [8]. The fibre itself presents a grade of anisotropy since the modulus of elasticity is totally different in the longitudinal direction of the fibre than in the radial one. It can be seen on the Table 2, which lists their main mechanical properties. Note that these can vary due to many causes; this table just provide generalized information to give an order of magnitude.

Table 2. Properties for high strength and high modulus carbon fibres [8]. Contrasted with [10] and [21].

Property	Symbol	Values for type of carbon fibre		Units
		High strength (HS)	*High modulus (HM)*	
Density	ρ	1.750	1.800	kg/m^3
Modulus of elasticity axial	E_l	230.000	390.000	MPa
Modulus of elasticity radial	E_r	15.000	6.000	MPa
Shear modulus	G	50.000	20.000	MPa
Poisson ration	ν	0,3	0,35	-
Tensile strength	σ_{rupt}	3.200	2.500	MPa
Useful Temperature limit	T_{max}	>1.500	>1.500	ºC

Generalizing, when the modulus of elasticity increases the strength decreases, resulting in more brittle fibres. High strength carbon fibres have still good stiffness and a better strength resistance. The rim studied is not a static part and it is subjected to impacts and fatigue, consequently it was chosen the high strength carbon for composing the material. This decision was supported looking into the choice of some bicycle wheels manufacturers [22].

3.2.4 Reinforcement-matrix mixture

Until now matrix and reinforcement has been presented separately. From now on it is going to be presented the mixture between both to form a composite material. Then, in order to work with a two phase material, it is useful to define some relations (one can define the same relations for the matrix phase):

- *Fibre mass fraction:* $M_f = \frac{Mass\ of\ fibers}{Total\ mass}$.
- *Fibre volume fraction:* $V_f = \frac{Volume\ of\ fibers}{Total\ volume}$.
- *Relation between M_f and V_f:* $M_f = \frac{V_f \rho_f}{V_f \rho_f + V_m \rho_m}$,

  where ρ_f and ρ_m are the densities of fibres and matrix respectively.
- *Mass density of a ply*[4]*:* $\rho = \frac{total\ mass}{total\ volume} = V_f \rho_f + V_m \rho_m$.

[4] A ply is the semi-product understood as the combination of reinforcements and the matrix in almost two-dimensional form [9]. It will be explained further in *Ply properties* section.

- *Ply thickness:*

It is said that a ply is treated as a two-dimensional product. Actually it has a small thickness that will be useful after to calculate the laminate thickness.

Denoting m_{of} the mass of fibre per square metre, the ply thickness *h* is:

$$h = \frac{m_{of}}{V_f \rho_f} \quad .$$

3.2.5 Isotropy and anisotropy

Composite materials are normally anisotropic. Their properties depend of the direction where they are tested. Sometimes, if the reinforcements are very short fibres or particles, they can be considered isotropic. Nonetheless composite materials with long fibres are usually highly anisotropic. They have planes of symmetry where their properties do not change along its normal orientations (along the fibre direction and transverse the fibre direction); therefore they can be particularized as orthotropic materials.

As it was seen on the continuum mechanics theories, one differential sphere deforms as an ellipsoid. The stress vectors also draw an ellipsoid. Then in an isotropic material the two ellipsoids, stress and strain ones, are coincident. Otherwise an anisotropic material does not deform in the same direction of the stress. There exists an angular distortion that separates the principal stress axes from the strain principal axes. Then the deformation ellipsoid is no longer aligned with the directions of the principal stresses. Figure 9 (a) illustrates this difference. Accordingly, in a macroscopic view, anisotropic (or orthotropic) materials deform in a different way than isotropic materials do, since also an angular distortion is involved. In (b) one can appreciate the different behaviour between two thin plates of isotropic and anisotropic material.

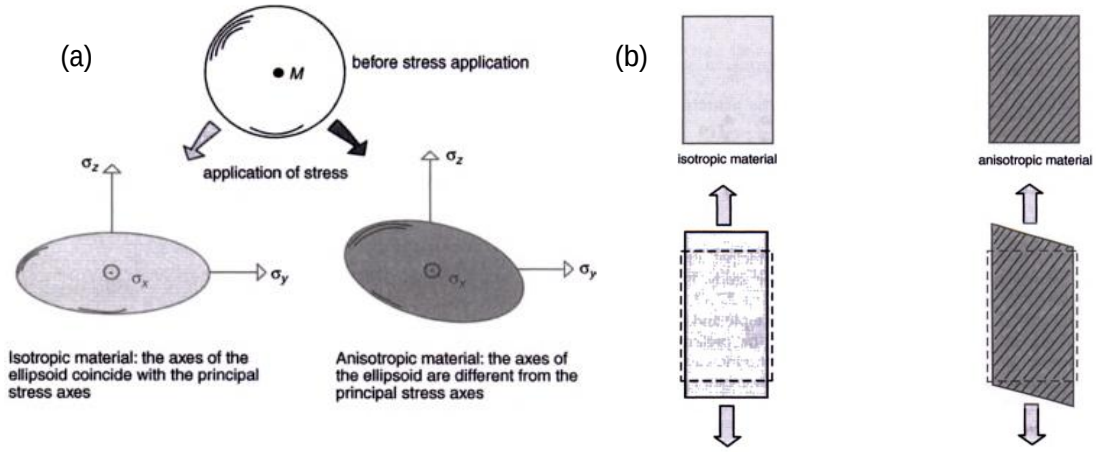

Figure 9. (a) Difference between the deformation ellipsoid on an isotropic and anisotropic material ([9]): On the top, the initial differential sphere, which deforms on an ellipsoid with the orientation of the axes of the principal stresses if it is an isotropic material (bottom left hand); or with an angular distortion in an anisotropic material (bottom right hand). (b) Comparison between the behaviour of a thin plate under tensile load, on the left an isotropic material and, on the right, an anisotropic one. [9].

3.2.6 Ply properties

A ply is the semi-product understood as the combination of the reinforcement and the matrix in almost two-dimensional form. With a certain amount of plies, which can be placed in different orientations, one obtains the laminate that will shape the final product. The plies are therefore the basis for understanding the composite material behaviour.

For carbon fibre reinforced polymers there are two basic forms of plies: unidirectional or woven fabric. These ones can be found in dry form or pre-impregnated with resin (pre-preg). They are presented in rolls form.

- *Unidirectional ply*

It was said that a ply is the minimum constituent for a composite material. If one knows the behaviour and the elastic constants for the unidirectional ply then it will be possible to know the mechanical characteristics of the laminate. The aim of this point is then to review the mechanical properties of unidirectional plies and present some approximate mathematical formulas for calculating them.

Figure 10 defines a general unidirectional ply. It also illustrates the transverse and longitudinal directions which will be used for defining its properties.

Hereinafter the subscripts *m* and *f* will be used to relate the magnitudes with the matrix and the fibre respectively. At the same time the subscripts *l* and *t* reference to the longitudinal and transverse directions of the unidirectional ply respectively.

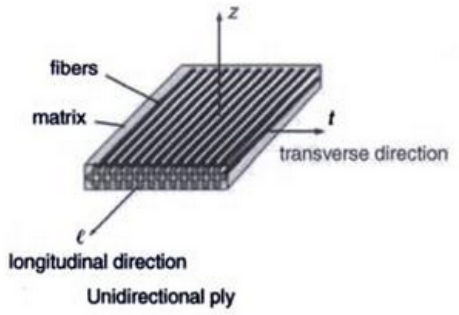

Figure 10. Components in a unidirectional ply and its orientations. [9]

Modulus of elasticity:

- Along the direction of the fibre E_l:

$$E_l = E_f V_f + E_m V_m = E_f V_f + E_m(1 - V_f) \quad .$$

- In the transverse direction to the fibre axis E_t:

$$E_t = E_m \left[\frac{1}{(1-V_f)+\frac{E_m}{E_{ft}}V_f} \right] \quad ,$$

where E_{ft} is the modulus of elasticity of the fibre along the transverse direction.

- Along an arbitrary direction:

In order to understand the great anisotropy that this type of materials exhibits, it is interesting to note how the modulus of elasticity decreases when the angle measured from the longitudinal axel of the fibres increases. This phenomenon is presented schematically on Figure 11. The mathematical formula for the modulus of elasticity along an arbitrary direction *x* is:

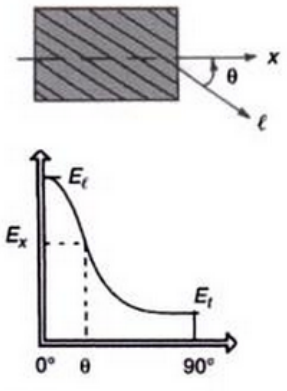

Figure 11. Relationship between modulus of elasticity and fibres' orientation. [9].

$$E_x(\theta) = \frac{1}{\frac{c^4}{E_l} + \frac{s^4}{E_t} + 2c^2s^2\left(\frac{1}{2G_{lt}} - \frac{\nu_{lt}}{E_l}\right)} \quad ,$$

where c = $cos\ (\theta)$ and s = $sin\ (\theta)$.

Shear modulus G_{lt}:

This is an approximation for the shear modulus of a ply:

$$G_{lt} = G_m\left[\frac{1}{(1 - V_f) + \frac{G_m}{G_{flt}}V_f}\right] \quad .$$

where G_{flt} represents the shear modulus of the fibre itself.

Poisson's ratio υ_{lt}:

It represents the contraction in the transverse direction *t* when a ply is subjected to tensile loading in the longitudinal direction *l*.

$$\upsilon_{lt} = \upsilon_f V_f + \upsilon_m V_m \quad .$$

Ultimate strength of a ply:

It is important to denote that a unidirectional ply made of CFRP does not yield. There is no plastic deformation when the ultimate strength is achieved, nevertheless the ply breaks.

The same phenomenon as the modulus elasticity occurs. The ultimate strength decrease when it is not measured in the reinforcement longitudinal direction.

When the fibres break before the matrix during loading along the fibres, an approximation is done:

$$\sigma_{l,rupture} \approx \sigma_{f,rupture} \times V_f$$

Then for an arbitrary direction, the ultimate strength is:

$$\sigma_{x,rupture}(\theta) = \frac{1}{\sqrt{\frac{c^4}{\sigma_{l,rupt.}^2} + \frac{s^4}{\sigma_{t,rupt.}^2} + \left(\frac{1}{\tau_{lt,rupt.}^2} - \frac{1}{\sigma_{l,rupt.}^2}\right)c^2s^2}} \quad ,$$

where *c* = $cos\ (\theta)$ and $s = sin\ (\theta)$. The fracture strength in the direction of the fibres is denoted as $\sigma_{l,rupt.}$, and in the transverse direction as $\sigma_{t,rupt.}$. Shear strength in the ply plane formed for the axis *l* and *t* is denoted as $\tau_{lt,\ rupt.}$.

Table 3 below summarizes the properties for unidirectional carbon fibre/epoxy plies. Note that these can vary with the manufacturing process and material choice. Since the table presents the properties of a ply with high-strenght carbon fibre, these will be used for the posterior calculations. If these properties actually provide a good approximation can be verified at the time of acquiring the final material (carbon fiber, epoxy).

Table 3. Properties of high strength carbon fibre /epoxy ply with V_f = 60% [9].

Property	Symbol	Values	Units
Specific mass	ρ	1.530	kg/m^3
Longitudinal tensile fracture strength	$\sigma_{l,rupt.(tensile)}$	1.270	MPa
Longitudinal compressive fracture strength	$\sigma_{l,rupt.(compressive)}$	1.130	MPa
Transverse tensile fracture strength	$\sigma_{t,rupt.(tensile)}$	42	MPa
Transverse compressive fracture strength	$\sigma_{t,rupt.(compressive)}$	141	MPa
In plane share strength	τ_{lt}	63	MPa
Interlaminar shear strength	$\tau_{interlaminar}$	90	MPa
Longitudinal elastic modulus	E_l	134.000	MPa
Transversal elastic modulus	E_t	7.000	MPa
Shear modulus	G_{lt}	4.200	MPa
Poisson ratio	ν_{lt}	0,25	-

- *Woven fabrics*

Woven fabrics are in fact unidirectional plies crossed perpendicularly. The two directions are called warp and fill. The fibres are woven together in different configurations, some of the more common are the ones presented on Figure 12 below.

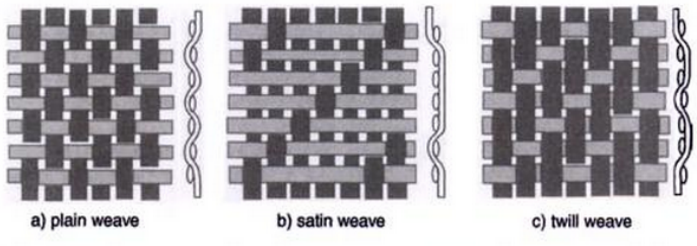

Figure 12. Three different types of woven fabric. [9].

For an approximation one can consider two crossed plies separately and apply the superposition theorem. Then one can calculate the mechanical properties and constants with the theory explained in the previous point.

The balanced fabrics are the ones which have the same number of yarns in the warp and fill orientations. For this type of fabric, the main properties are listed in the Table 4 below. As well as the other tables of properties exposed before, the values of the properties can vary. Nevertheless, it is thought to be a good approximation and will be used for further calculations. As it was said for the properties of unidirectional plies, these can be verified at the purchase moment.

Table 4. Properties of carbon balanced fabric/epoxy. V_f = 45%. [9].

Property	Symbol	Values	Units
Fibre volume fraction	V_f	45	%
Specific mass	ρ	1.450	kg/m^3
Tensile fracture strength along x or y.	$\sigma_{rupt(tensile)}$	420	MPa
Compressive fracture strength along x or y.	$\sigma_{rupt(compresive)}$	360	MPa

In plane shear strength	τ	55	MPa
Elastic modulus	E_x=E_y	54.000	MPa
Shear modulus	G_{xy}	4.000	MPa
Poisson coefficient	ν_{xy}	0,45	-

3.2.7 The laminate

How to calculate the ply characteristics was exposed in some of the points before. Nevertheless, the plies are only the basic element that one has to understand in order to work with the laminates. The laminate is formed stacking up oriented plies. The designer has to choose how many plies are needed and its orientations. It is the versatility of the composite materials that make sizing the laminate the most important part of the design.

Ply orientation

When the loads are known, one can adapt the relative position of the layers against the loads in order to resist it more efficiently. The favourable configuration is when the fibres orientation is the same or near the normal stresses direction, and more specifically on the principal stresses directions. In this way, the fibres are supporting the main loads. Moreover the matrix cannot resist too much stress, then one has to avoid the configuration where the fibres are transversal to the normal stress, in this case it is actually the resin that is resisting the load. The shear stress is as well dangerous for the matrix and to cause delamination that is the separation of different plies [12].

Due to the high anisotropy that composite materials presents, and for a matter of safety, it is important orientate a minimum number of plies (a ten percent minimum according with [16]) in the main directions. Main directions are considered 0º (the main load axis), +45º, -45º, 90º (transverse to the main load axis). Nevertheless, depending on the application and the case of study these orientations can change.

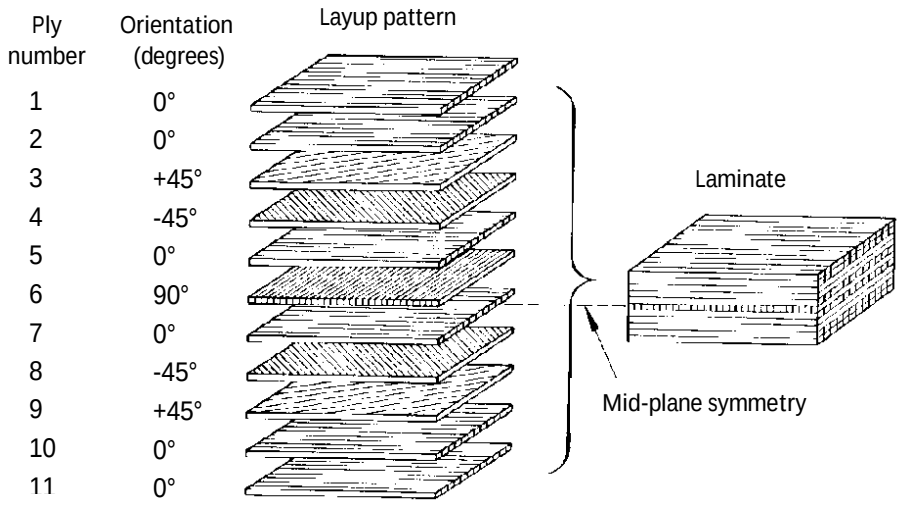

Figure 13. Example of laminate configuration with mid-plane symmetry. Each ply can be oriented differently in order to achieve different properties.

Layup notation

In order to describe a laminate, it will be used one notation to do it [23]. For the example in Figure 13, the notation would be:

$$(0_2/45/\text{-}45/0/\overline{90})_s \quad ,$$

where the '2' denotes that there are two consecutive plies in the 0° orientation and the '*s*' denotes that there is a mid-plane symmetry. There is a bar over the '90' to denote that it is the middle plane.

To represent a woven fabric oriented at 0°\90°, an *'F'* would be placed next to the ply to indicate it, as *90F* or *0F* indistinctly.

3.2.8 Failure of laminates

Failure criterions

The strength of materials can be predicted based on different failure criteria. One failure criterion tries to relate the material strength, defined for uniaxial tension-compression and shear, with the general stress-strain state due to loads. Failure criteria can be presented as mathematical expressions called failure criterion functions *(f)*:

$$f = function\,(stresses\ or\ strains, material\ strength) \quad ,$$

where f ≥1 indicates failure.

Since the failure function is not a linear equation, the value of the function does not tell the real distance to the failure point [24]. Then the reserve factor (RF) is used. It tells the actual distance to the failure point from the point represented by the applied load. The reserve factor (RF) indicates margin to failure. The applied load multiplied for the reserve factor gives the failure load:

$$RF \times F_{applied} = F_{failure} \quad .$$

Reserve factor values greater than one indicate positive margin to failure and values less than one indicate negative margin. The values of reserve factors are always greater than zero. For high performance applications, as the case on study, it is preferred to leave an adjusted safety margin for no oversize the design [16]. In this thesis the part designed seeks to be as light as possible but maintaining the safety, on the border between performance and security. For these reasons the reserve factors over 1,5 will be accepted. Reserve factors much bigger should be avoided since it is a signal that the part is oversized.

Tsai-Hill failure criterion

The damages on composite materials are a bit different than in common materials. For laminates, one cannot use typical failure criterions as Von Mises failure criterion because it is not only about the value of the stress since the material orientation and other factors are as well crucial parameters, as it was explained on section *Isotropy and Anisotropy*.

Therefore some failure criterions have been developed specifically for the composite materials. One of the firsts to do it was Hill on [25], with an adaptation of the Von Mises failure criterion [26] for anisotropic materials. These criterions are based in the distortional energy

which consider the failure of the material when a critical amount of distortional energy is achieved. Few years later Tsai and Wu developed their criterion; it is explained in [27].

In this thesis the failure criterion used is the Tsai-Hill failure criterion [28] which is a simplification of the Tsai-Wu failure criterion. Hill, Tsai-Wu and Tsai-Hill failure criterions are included on the quadratic failure criterions set. In a quadratic criterion all the stress or strain components are combined into one expression. The general form of quadratic criteria can be expressed as a second-degree polynomial.

The Tsai-Hill number is one of the most commons failure criterion used for design calculations on composites materials [12]. This criterion has to be used at each ply separately. Here is presented in a two-dimensional form, for each ply:

$$\alpha^2 = \left(\frac{\sigma_l}{\sigma_{l,rupture}}\right)^2 + \left(\frac{\sigma_t}{\sigma_{t,rupture}}\right)^2 - \frac{\sigma_l \sigma_t}{\sigma_{l,rupture}^2} + \left(\frac{\tau_{lt}}{\tau_{lt,rupture}}\right)^2,$$

and the Tsai-Hill number 'α' denotes:

- If α<1: the ply does not break
- If α>1: rupture occurs in the studied ply. It does not mean that the laminate will break.

Note that the ultimate stress in a longitudinal ($\sigma_{l,rupture}$) and transverse direction ($\sigma_{t,rupture}$) could be different in tensile and compressive strength. Then depending on the load case one has to put the related one.

The failure criterion exposed above is in a two-dimensional form since only longitudinal and transversal directions are considered. Nevertheless, sometimes The Tsai-Hill failure criterion can be used in a three dimensional form, it is presented in the appendix D.

3.3 Finite Element Method

The finite element method (FEM) is a numerical procedure for obtaining solutions to the differential equations that describe, or approximately describe a wide variety of physical problems like solid mechanics, electromagnetism, fluid dynamics, heat transfer inter alia.

3.3.1 History

The finite element method was developed as we know nowadays, during the 60s and 70s and its origins are in aircraft structural engineering. But before that, three research groups had imposed the mathematic bases for the posterior development of the method. They were the mathematician R. Courant, the physicist J.L. Synge and the engineers J.H. Argyris and S. Kelsey.

Many names contribute to develop and expand the FEM, some of the pioneers were M. J. Turner and L.J Topp engineers from Boeing company, R. W. Clough from UC Berkeley (how define the method as finite element method) , H. C. Martin from the University of Washington. They publicized together the article "*Stiffness and deflection analysis of complex structures*" in 1956 [29] which is the first formal presentation of the method.

3.3.2 Basics

The underlying premise of the method states that a complicated domain can be sub-divided into a series of smaller regions in which the differential equations that govern the physical

problem are approximately solved. By assembling the set of equations for each region, the behaviour over the entire problem domain is determined. Each small subdivision is referred to as an element and the process of subdividing a domain into a finite number of elements is referred to as discretization. Elements are connected at specific points, called nodes, and the assembly process requires that the solution be continuous along common boundaries of adjacent elements.

When confronting a physical problem, the governing equations for the phenomenon are usually known. But often the geometry and configuration of the problem is too complicated to solve the equations by hand. This is the reason why we use the Finite Element Analysis (FEA) that applies the finite element method. There is a variety of FEA software, but in this thesis we are going to use ANSYS 15®.

3.3.3 Steps in the finite element analysis

An overview of the functioning of the finite element analysis would be done in this point [30]. The explanation will focus on the variant of the method used for solving solid elasticity problems. We assume that the geometry of the problem is already created; it can be modelled with a CAD program.

Pre-processing phase

When we have the geometry the first step is to discretize the domain in a finite number of elements. This operation takes the name of meshing. Figure 14 illustrates the meshing process, which divides the geometry in small elements connected with each other through nodes. The mesh is a determining factor to achieve accurate results, more forward will be discussed how to control its quality.

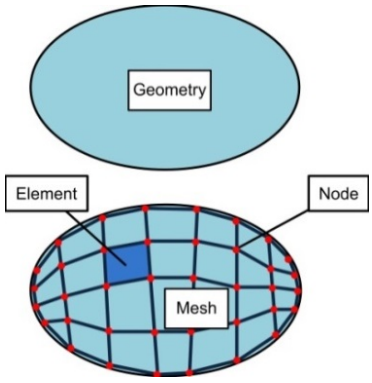

Figure 14. Discretization of a domain through a mesh; elements are the divisions, interconnected using nodes.

Then one has to assume a shape function to represent the physical behaviour of element. It has to be a continuous function that has to be able to solve the element behaviour.
In elastic problems, it is the relation between the stress and the strain explained by Hooke's law,

$$F = ku \quad ,$$

where, defined between two nodes, F and u are the force and the displacement between both respectively and k is the elastic constant of the material.

After that, all the elements are assembled to present the entire problem. It is reflected with the creation of the global stiffness matrix *[K]*. This matrix represents the geometric arrangement of the problem as well as the physical properties of the elements.

Now the boundary conditions, initial conditions and loads are applied. It can be prefixed displacements, pressures, forces, heat flows, etc. The displacements are expressed in one matrix *{U}*, where each component is the displacement of one node. There is also the matrix of applied external loads *{F}*.

One can see this set of equations, reflected in matrixes, as:

$$\{load\ matrix\} = [stiffness\ matrix]\{displacement\ matrix\} \quad ,$$

or:

$$\{F\} = [K]\{U\} \quad .$$

Solution phase

The problem is now defined by usually large system of linear or nonlinear algebraic equations. It has to be solved simultaneously to obtain nodal results, such as displacement values in elastic problems or temperatures in a heat transfer problems.

Here is where the computer gives us an advantage, it isolates the *{U}* matrix and solves the following system,

$$\{U\} = [K]^{-1}\{F\} \quad .$$

Post-processing phase

Known displacements, with the appropriate transformations one can find other important information that may be of interest. That could be the stresses (principals, shear, etc.), failure points, safety factor or what needed.

3.3.4 Quality measures for mesh

The mesh can influence a lot to achieving accurate results in simulations. There exists different quality mesh metrics that help us to distinct a good mesh from a bad one. During the present work the quality mesh metric used will be the skewness.

Skewness

Skewness is a quality measure for a mesh that gives us information about how close to ideals are the elements [24]. Specifically, it compares each face of the element with its ideal face. For example, if the mesh is done with hexahedrons, the skewness measures how large are the angular distortion of the six rectangular faces approaching the ideal equiangular rectangular faces. Figure 15 represents this phenomenon with a triangular and rectangular faces.

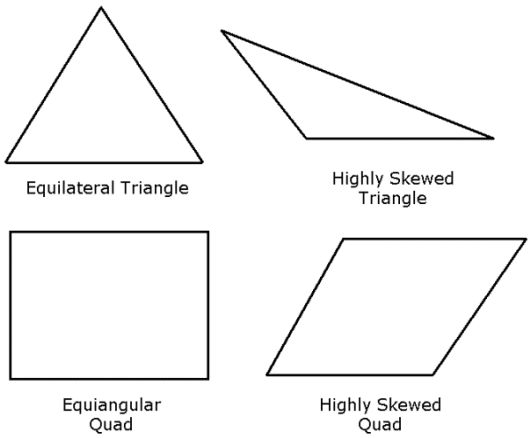

Figure 15. Comparison between ideal and skewed faces. [24].

The Table 5 below illustrates the ranges for the skewness and the respectively face quality.

Table 5. Range of skewness values and corresponding cell quality. [24] .

Value of Skewness	Face Quality
1	degenerate
0,9 – <1	bad
0,75 – 0,9	poor
0,5 – 0,75	fair
0,25 – 0,5	good
>0 – 0,25	excellent
0	equilateral

Highly skewed faces and cells (high values of skewness) are unacceptable because the equations being solved assume that the cells are relatively equilateral or equiangular, depending on the element type.

The skewness is going to be used in the present thesis to control the mesh quality during finite element analysis. The controlled value is rather the average skewness of all elements of the model.

3.3.5 Application in composite materials

Composite materials are somewhat more difficult to model than an isotropic material such as aluminium or steel. That is because each layer may have different properties. Although there are some element's types that allow layered materials.

ANSYS® 15 allow us to use a group of specialized elements for composite materials called *Layered elements*. These ones are the SHELL181 and 281, SOLSH190 and SOLID185 and 186 layered solid. In some parts of this thesis the element SHELL181 is going to be used for validating the layered parts, then here it is going to be explained further its characteristics [24].

A shell type element is a two-dimensional element that can contain information of a thickness. Then one can simulate three-dimensional parts using a two-dimensional element, with the reduction of calculations that it entails.

SHELL181 is suitable for analysing thin to moderately-thick shell structures. It is a four-node element with six degrees of freedom at each node: translations in the x, y, and z directions, and rotations about the x, y, and z-axes. SHELL181 is well-suited for linear, large rotation, and/or large strain nonlinear applications. This element can be used for layered applications, for modelling composite shells or sandwich constructions. The accuracy in modelling composite shells is governed by the first-order shear-deformation theory (usually referred to as Mindlin-Reissner shell theory. See [31] and [32]).

4 Requirements and previous calculations

Before starting the design, the requirements that the rim had to accomplish were reviewed. Moreover the necessary calculations were also done, in order to know the loads that the rim would have to withstand.

4.1 Requirements

The design of the rim must follow the Shell Eco-marathon® rules [33]. For the 2014 rules, any restriction exists on the wheels and rims field. Nevertheless, considering that the tires are already selected for the HiGtech team, the rim must follow the tire manufacturer specifications. In that case the rim main sizes are determined.

The tires[5], supplied by Michelin, have a very low rolling resistance[6] (C_{rr}=0,001), if it is compared with typical bicycle tires (inflated around the same pressure) which have coefficients around 0,005. Other technical specifications are the maximum pressure of 7 bars (0,7 MPa), load capacity of 100 kg and the speed limit for 70 km/h, these fit perfectly with the Shell Eco-marathon® vehicles characteristics. It can be assembled with standard tube or in a tubeless way (see Figure 16). The overall diameter is 478 mm.

The rim's recommended dimensions for the selected tire are listed in Table 6. Representation of these can be seen in Figure 16.

Table 6. Rim dimensions for Michelin 45/75 R16 tires.

Measurement	**A**	**B**		**G**	**P**	**H**	**C**	**R1**	**R2**	**R3**	**R4**	**R9**	**D**	**πd**
Tolerance limits	+0,15 -0,5	min.	max.	±0,5	+0,2 -0	+0,1 -0,5	ref.	ref.	max.	min.	min.	min.	-	+0,2 -0,5
Values	34,0	6,5	8,5	10	3,5	7,5	4	6,5	1,5	2	5	7	405,6	1.274,2

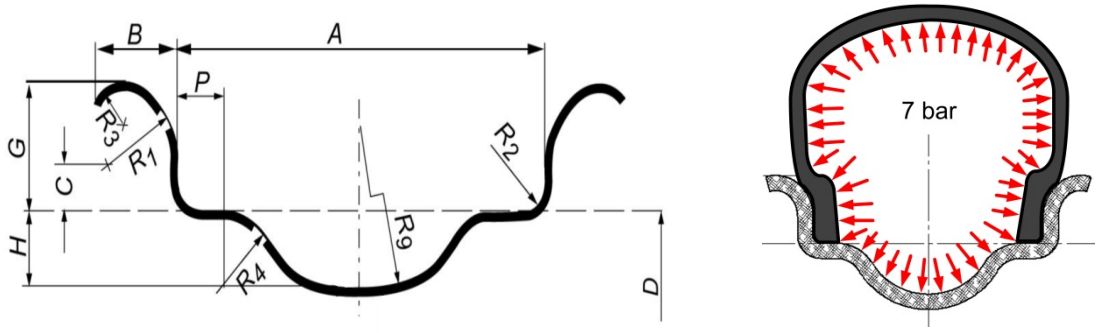

Figure 16. On the left, sketch of the contour. On the right, illustration of a tubeless tire mounted on the contour.

[5] Michelin 45/75 R16, for prototype vehicles.
[6] Dimensionless coefficient that relates the rolling resistance force with the normal force, the force perpendicular to the surface on which the wheel is rolling.

4.2 Loads determination

There are four main types of loads acting on the rim:

- Torque on the shaft axis. Caused mainly for the braking situations (prevailing over the torque caused on the acceleration situation).
- Radial forces. They can be caused for different situations, like the vehicle weight itself, the driver ingress in the vehicle, and the irregularities of the road.
- Lateral forces. They occurs mainly on the cornering situations, induce normal and lateral load components on the rim.
- Pressure. The special tires are inflated at high pressures that are applied on the outer surface of the rim's contour.

In order to find the values for each of these loads, an analytic study for the different cases was done. Previously, the main vehicles characteristics were looked for. The weight of the vehicle plus the driver was estimated in 100 kg, with the distribution of 30 kg on each of the front wheels and 40 kg on the rear wheel (on a flat ground). The location of the centre of mass and other main magnitudes are summarized in the Figure *17*.

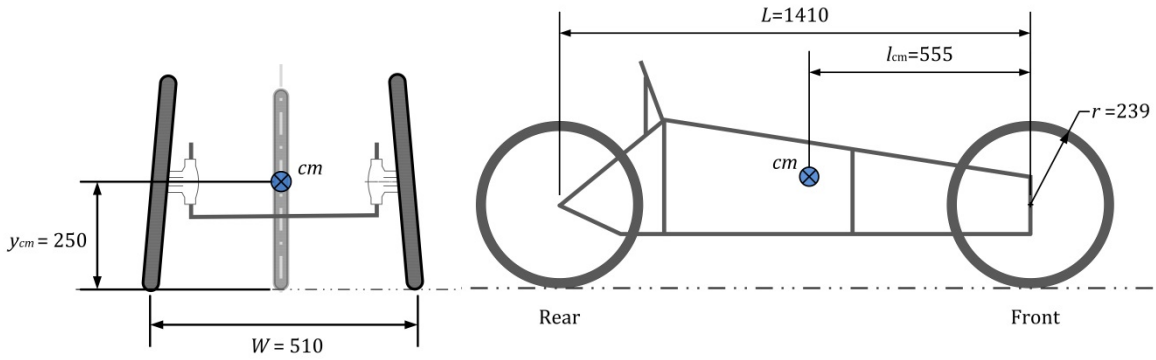

Figure 17. On the left, front view of the vehicle. On the right, at other scale, the side view. Main dimensions in millimetres and, in blue, the centre of mass, cm.

The calculations will be divided into three different situations, the braking situation, the cornering situation, and the driver's ingress on the vehicle. They are considered the more adverse situations.

4.2.1 Braking situation

The only two situations that induce a torque on the rim are the braking and the acceleration cases. Due to the characteristics of the vehicle (without great accelerations on its driving) the acceleration torque is not as high. Therefore only the braking case was studied.

The two situations studied were the regulated braking test that the vehicle has to pass before the competition, and an emergency braking situation. When one uses the brake system, it applies force on a brake disc united with the rim's hub. Therefore the brake situation produces a torque on the hub that is transmitted on the entire rim.

Braking test

It is a rule that the vehicles have to be provided with two independent braking systems (front and rear). In the braking test each system alone has to be able to keep the vehicle immobile on a 20% inclined slope (11,3°). In this case, the rear wheel is the one which has to support the highest braking force, since the front brake system shares the loads between two wheels.

For this case the torque obtained in the hub of rear wheel is:

$$\Gamma_{braking\ 1} = mg\sin(11{,}3°) \cdot r = 46\ Nm \quad .$$

where *m* is the mass of the vehicle, *g* the gravity constant, and *r* the radius from the rim axis of the rim to the external part of the tire touching the ground.

Emergency braking

The vehicle in study doesn't incorporate anti-lock braking system (ABS) so in an emergency braking wheels become locked. It is assumed that the locked wheel slides on an emergency brake situation. Therefore the calculations, the kinetic friction coefficient has to be taken into account. Considering a dry asphalt and low friction rubber, the kinetic friction coefficient will be approximated to 0,7 [7]. Note that the track on the competition is flat, thus it is also considered a flat ground.

There are three possibilities for the emergency braking situation, considering that the two front wheels always brake at the same time. These are: the three wheels braking at the same time, only the front wheels or only the rear wheel. The worst scenario is when only the rear wheel is braking since only one wheel is doing the force. This is the situation explained below.

The weight small displacement between the rear and the front parts of the vehicle on a braking situation can be neglected, due to the low centre of mass and the absence of suspensions. The kinetic frictional coefficient is considered constant. Therefore the frictional force maintain constant,

$$F_{friction} = \mu_k N_r = 275\ N \quad ,$$

where N_r is the normal force acting on the rear wheel. The frictional force induce a torque on the hub which is transmitted through the rim, the value is:

$$\Gamma_{braking\ 2} = F_{friction} \cdot r = 66\ Nm \quad .$$

Note that if one speaks only in terms of forces, the time the vehicle will take to stop and the initial velocity are not relevant.

The emergency braking situation puts the rim on higher efforts than the braking tests. For this reason the loads found would be considered later for the posterior dimensioning of the rim.

[7] Source: http://www.engineering toolbox.com & http://hpwizard.com

4.2.2 Cornering situation

While cornering, the weight distribution changes. The centripetal force tends to overturn the vehicle and it charges more the outer wheel, increasing the radial force as well as the lateral load. The limit case is before the overturn, when the inner wheel stops touching the ground. Figure 18 draws the free body diagram for this situation. The centripetal force, which causes the overturn, is defined as

$$F_c = \frac{mv^2}{R},$$

where R is the turn radius of the corner, v the vehicle's velocity, and m its mass. Just before the overturn, for equilibrium of moments,

$$F_c \cdot y_{cm} = mg \cdot X_{cm}$$

where X_{cm} is the distance between the centre of mass and an imaginary overturn line. Note that the inner wheel has not normal force neither friction force, since it is the moment just before the overturn and the wheel is not touching the floor. Considering a turning velocity of 30 km/h, then the minimum turn radius before the overturn is approximately 12 metres.

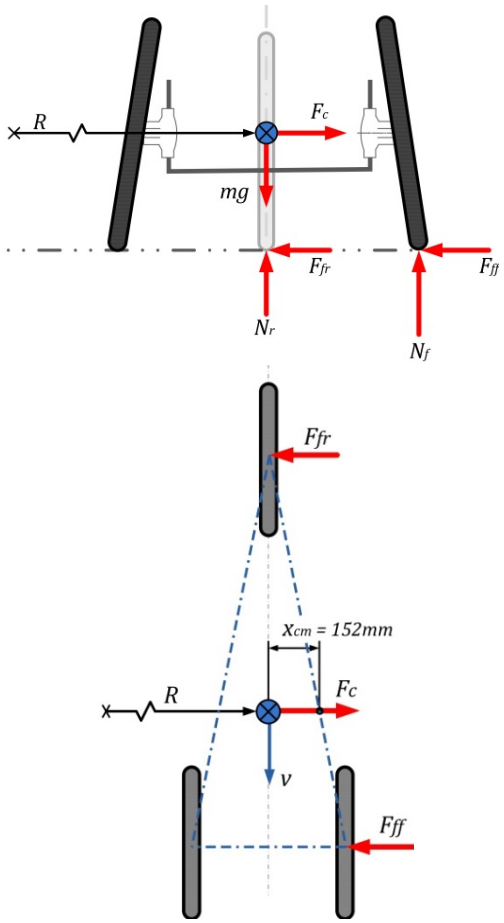

Figure 18. Free body diagrams: Main forces acting when cornering, just before overturn. On the upper side, the front view; on down side, the top view at a different scale. X_{cm} in millimetres.

Studying this situation the centripetal force is F_c=578 N, then assuming that any wheel is sliding, the highest lateral force is presented on the outer front wheel, F_{ff}=228N. The maximum normal force is as well higher on the front wheel, because the interior one has not normal force when the overturn is imminent. Then the normal force increase in the outer wheel, N_f=589 N.

4.2.3 Static situation & driver's ingress

The estimated weight distribution for the vehicle is 60 kg in the two front wheels and 40 kg in the rear wheel (with the driver inside). It means that in static condition the rear wheel will support approximately 400 N. There will be situations where the load will be higher like in the cornering case seen before.

Another case studied is when the driver ingress into the vehicle. The driver puts her/his feet on the front part of the chassis. Then only the front wheels are holding the driver's weight. In this situation, each front wheel is holding approximately also 400 N.

Thus the maximum radial force occurs when cornering.

5 Design of the rim

This chapter explain the development process followed when designing the rim and the results achieved during it. The final design validation is also presented. To finish, the integration of the rim on the vehicle and a possible method of manufacture are studied.

5.1 Design process

The design process started with choosing a preliminary design, which defines the profile for the rim. Then this profile was optimized and the final dimensions were defined. The stress state of the rim was analysed, founding the principal stresses and its orientations. This information was then used for sizing the laminate.

The process was mainly supported for finite element analysis; due to the complex geometry of the rim an analytical analysis was not a viable option. It helped to find the optimal shape, via a statistical optimization method and also to find the stresses on the rim.

5.1.1 Preliminary design

The preliminary design wanted to find a starting concept profile. Without determining neither dimensions nor characteristics, but thinking about the final rim and the viability of the concept. Many solutions were valid to solve this problem and the job was to discard expensive, non-viable and bad solutions. For that purpose a review on the related literature was done in order to discard bad options and focus on the good and more tested ones.

Profile

Regarding the shape or profile of the rim, one of the most important things to take into account is that the wheel has to withstand lateral forces. Differing from a bicycle wheel that while turning is inclined, so it resists the loads mostly in a radially form; in our case of study, the wheel will be always vertical also in the cornering, it means that the lateral force has to be resisted by the rim laterally.

In order to acquire an overview of the more viable options, some related literature was revised. Due to the manufacturing process, the rim's profiles used for this kind of vehicles are usually closed profiles, the more tested are the L, U, and V profiles (referring to its shape, see Figure 19). The lateral stiffness was tested and compared between profiles in [12] and [13] and both coincide that the V profile has the highest lateral stiffness, and supports better the lateral load. The V profile is based on a triangular structure which is widely known for withstanding loadings without too much deformation. When the lengths of the sides are fixed, the angle between the sides is restrained. It shears out the loads through the structure in compression and tension forms. This phenomenon is illustrated in the Figure 19, which also shows the tendency to bend that the other profiles have.

Therefore the V profile was selected for further optimizations and follows the design process.

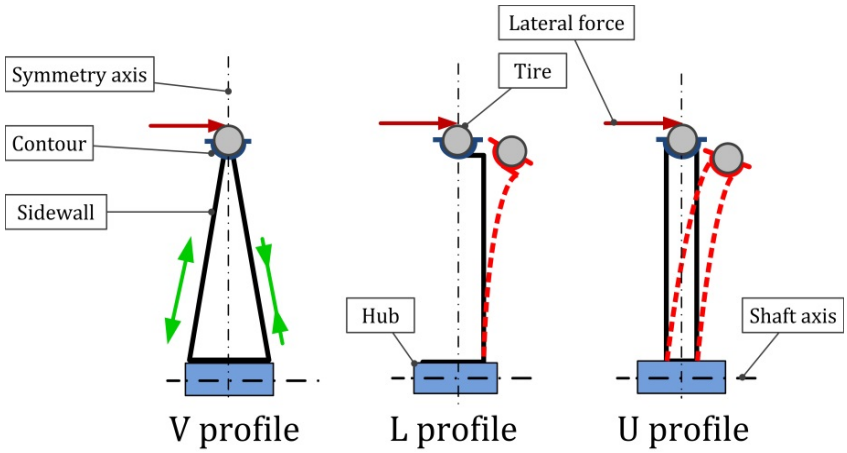

Figure 19. Three different rims profiles (section view). The V profile tends to resist the lateral load with compressive and tensile stresses on the sidewalls (in green). The L and U profiles tend to bend due to the lateral load (exaggerated bended shape in red).

The V profile also has a good aerodynamics [34]. Nonetheless this is not fundamental in this case of study due to the fact that the wheels are covered with the vehicle body and they do not change the vehicle drag force. Anyway it could be useful in the future if the team decide to place the wheels outside the body.

Parts of the assembly

The three wheels of the vehicle will be equal in order to achieve an easier fabrication, since the same moulds would be used for manufacturing process of the three wheels. It means that the fabrication price, that represents a high percentage of the whole price, will be lower.

Since the high air pressure inside the tire is supported for the contour, it was considered to separate the rim into three different bodies, the contour and the two symmetrical sidewalls (see V profile in Figure 19). It would be possible to design the contour with more thickness and stiffness for supporting the air pressure.

Finally the V profile formed with three parts (contour plus two sidewalls) was chosen for latest detail designs and optimizations. This decision was based in aspects like the easiness of the fabrication process, the good aerodynamics and the good stiffness compared with the other designs.

5.1.2 Boundary conditions for the simulations

The next steps in the design process implicate FEA simulations. This point wants to present the boundary conditions used and how were applied on the model.

The boundary conditions represent how the simulated model interacts with the environment. These are the loads and the subjections or constraints that will be applied on the rim in order to achieve a simulation as near as possible from the reality.

Loads

Although the values of the loads are known, the application of these ones on the rim is quite difficult. The tire, which is the element that leads the loads between the ground and the rim, has a complex and mostly unknown behaviour. To solving this uncertainty, one simplification was accepted. The loads were applied in a 20 degrees sector of the contour of the rim which

was assimilated as the zone where the tire would transmit the loads. The air pressure was applied on the entire contour external surface. Figure 20 below shows where the loads were applied on the rim.

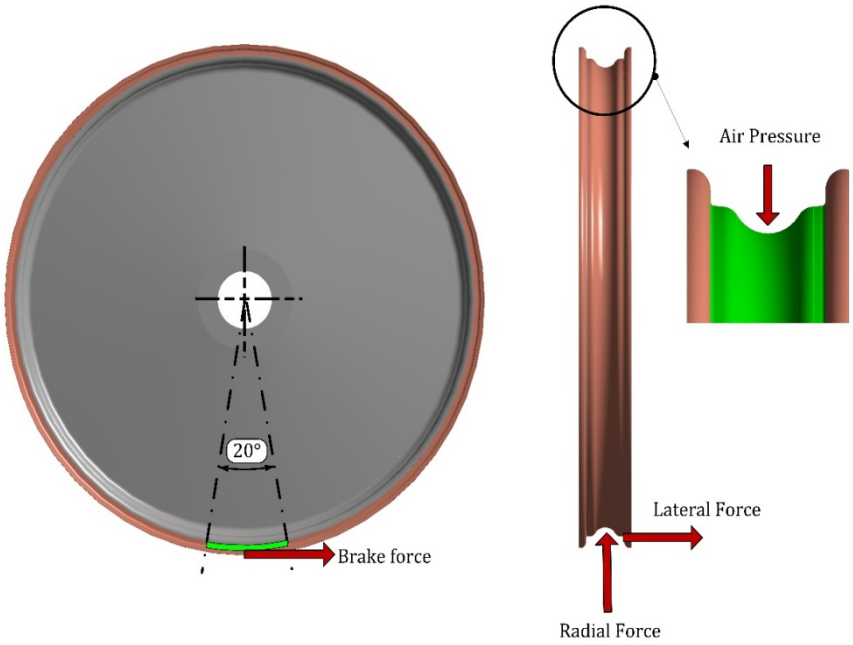

Figure 20. In green, areas of application of the different loads on the simulated models.

The values of the forces applied on the model are the ones found on the analytical study multiplied by the safety factor, they are listed in Table 7 below. A safety factor of 1,5 was used for dimensioning. The reason for using a safety factor is to avoid any uncertainty in the loads determination, since there are factors in the analytic analysis that are not controlled.

Table 7. Loads applied on the model during the design process and validation.

Type of load	Value with safety factor	Units
Radial Force	883,5	N
Lateral Force	342	N
Brake Force	412,5	N
Air pressure	1,05	MPa

Constraints

In order to carry out a static structural simulation for the rim, one has to restrain all the six degrees of freedom that it has as a rigid body. If it is not done correctly, the element could have free motion and the results of the simulation would not be trustworthy.

Locking the steering mechanism that induce one degree of freedom on the wheel , the wheel itself only has one degree of freedom since it can only rotate around the shaft. The rim is joined together with the hub. Then the hub through the bearings can rotate around the shaft. Brakes and the engine are responsible of controlling the only degree of freedom of the wheel (the one in the rear), always through the hub.

For these reasons the constraint was applied locking the cylindrical contact of the rim with the hub, restraining the spin of the wheel.

5.1.3 Determination of the shapes

This point presents the process for dimensioning the rim's profile. Using the concept of the preliminary design, an approximate design was modelled with aluminium alloy, and then it was simulated and optimised. It was done in two stages, first only the contour was simulated, loaded with the pressure of the air. Then when the contour was already optimized, it was assembled with the sidewalls to optimize these ones.

Introduction of the optimization process

The procedure starts selecting *k* parameters, the ones which one wants to study. These input parameters can be for example physical properties or dimensions from the sketch. At the same time one has to know which response objectives, output parameters, wants to optimize. In this case the response parameters would be stresses.

Using the method of design of experiments (DOE), a factorial experiment is designed [15]. It consists in choosing *p* values, or levels, for each input parameter *k*, and creates all the model's combinations (p^k samples) between them. Each sample has a particular combination of the input parameters. Then testing each sample and recollecting the response values one can know the effect of each parameter on the response, and also the effect of the interaction between parameters on the response. One way to visualize the results is via the response surface [14]. The response surface is the representation of the response in function of the input parameters.

Contour definition

The contour is one of the most important parts of the rim and it is subjected to high loads due to the air pressure. For the optimization process, it was modelled without the sidewalls; it reduces the complexity of the simulation achieving similar results since only the shape was looked at.

First the input and response parameters were chosen. As one can see in Figure 16, on the specifications for the rim, most of the parameters have a fixed value or a reference value. For these reason only the *R9* parameter was entered as an input parameter since it is the one which changes the shape of the contour significantly. Note that *R4* and *R9* are directly related since *H*, *P* and *A* are fixed values. Then it is only necessary to study one of them. The parameter was limited with an upper limit of 11 mm and a lower limit of 7 mm, for geometric reasons it cannot be higher or lower that these. The response objective was the first principal stress. It is studied because gives us an idea of the state of stress on the contour, and the other stresses are, in some way, related with the magnitude of this one. It is a threatening tension in the outer side of the contour due to bending, as it will be seen in the results.

The study was carried out with a two degrees sector of the contour, due to the cyclic symmetry. Taking also advantage of the mirror symmetry only half part of the contour was simulated. The contour thickness parameter was fixed in 3,5 mm. This parameter depends on the number of plies that the final laminate will have, so this is just an approximation. Another thing to take into account is the fact that the simulation is done without the sidewalls supports. Then only the contour is withstanding the bending moment produced by the air pressure, and the stress values would be higher.

The mesh was controlled in the entire contour to ensure that the results were more accurate, achieving an average skewness of 0,185. The pressure was applied in the top surface with a safety factor of 1,5 (0,7MPa x 1,5).

As Figure 21 shows, the maximums for the principal stress are located in the middle of the contour. Due to the bending moment that the air pressure induces on the contour, the higher tensile stresses are located on the outer part. Figure 21 shows the effect that parameter R9 has on the response. The principal stress decreases lineally as the R9 radius increases. For these reasons R9 was fixed at 11 mm.

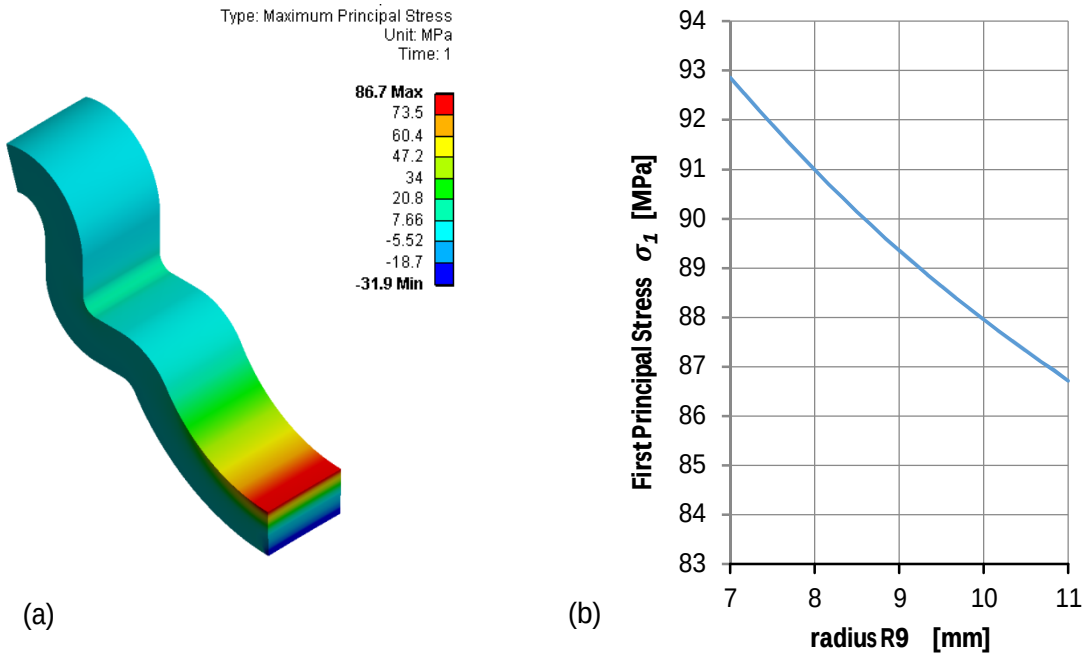

Figure 21. (a) Location on the contour model of the first principal stresses. Parameter R9 fixed at 11mm. (b) First principal stress versus the radious R9, as a changing parameter.

The final shape for the contour is drawn in the Figure 22 below. This figure also defines the coordinate system that will be used later. The contour thickness could not be known at that point since the determination of the number of plies was necessary.

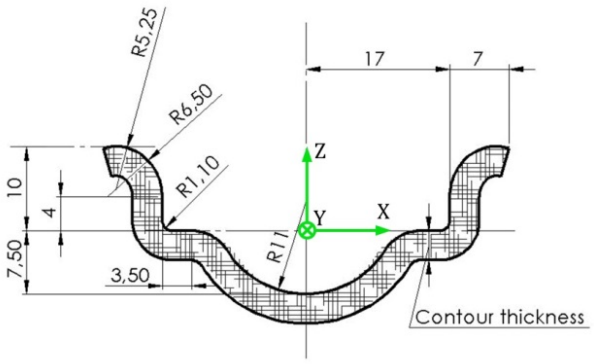

Figure 22. Final dimensions for the contour. Values in millimetres. In green, the contour's coordinate system.

Sidewalls definition

The optimization of the sidewall aimed principally to find the best sidewall angle for withstand balanced the lateral and radial forces. Some parts of the sidewalls were already defined. The upper part of the sidewall has to follow the contour shape since the contact between both parts will be glued. The same happens with the lower part, which is in contact with the hub.

The loads applied for the optimization were the lateral and radial force, since the objective was to find the best profile to withstand these ones. The brake force induces a torque in the entire rim that is supported for all the sidewall, but the shape of the profile is not that significant in this case. The air pressure was not applied on the contour, since it has the same effect on the lateral and radial force case and then it is not necessary. Then the study was divided in the two cases, lateral and radial forces. The optimization looked for an optimum point for both.

- Rim's model

The simulation of these two cases implies non-symmetric loads. Thereupon one cannot simplify the geometry simulating only a sector of the rim (as it was done in the contour optimization). The only possible simplification was to simulate only half rim and apply mirror symmetry condition in the cutting area.

As it was explained in the boundary conditions section, the loads were applied in a ten degrees sector in the bottom of the model, since only half rim was simulated.

To restraint the free movement, the model was fixed through the cylindrical support with the hub.

The mesh was carefully defined for achieving less consuming time in the simulations but also accurate results (see Figure 23). Finally an average skewness of 0,2471 was achieved, a quite good value according to Table 5 presented on the theories (see section 3.3.4).

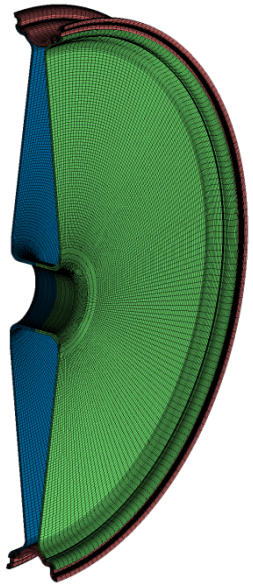

Figure 23. Mesh of the half rim model. In green and blue the two sidewalls; in red the contour.

- Input parameters for the optimisation

Two parameters were chosen for the sidewall optimization, both represented in Figure 24. On one hand the *S* parameter, this controls the angle of the sidewall. If *S* decrease the angle is more pronounced. On the other hand the radius *R*, at the upper part of the sidewalls. It was thought to be an important parameter to control since the connection with the contour is a crucial point. Other dimensions like the sidewall thickness was approached to a sensible value since it was unknown by that moment (it depends on the laminate thickness).

The *S* and *R* parameters were limited in high and low levels. Although they are continuous variables, a limitation was

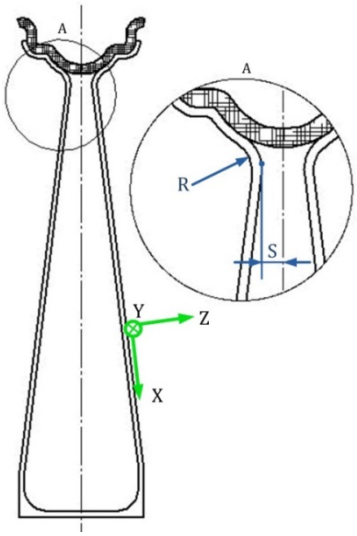

Figure 24. Definition of the R and S parameters. In green, the coordinate system for the sidewalls.

necessary. It was done due to some geometrical limitations. For example, if *R* becomes very big, the contact area between the contour and the sidewalls is reduced, and then the bonding would be weaker. For the *S* parameter is more or less the same, if *S* is very big, the bonding area becomes reduced also. It has no sense than the *S* parameter becomes very small since the two sidewalls would be almost touching each other; in this case the capacity for balancing the forces becomes reduced.

Then the table of experiments could be done. Three values of each parameter are picked, the high and low limits of the parameters and an intermediate value between those ones; they are listed on Table 8. The resultant factorial design is a 3^2 with nine samples, since it has three levels for the both parameters.

Table 8. Levels for each parameter on the sidewalls optimization.

Parameters	**Levels [mm]**		
	Low	Intermediate	High
S	3	5	7
R	5	7	9

- Response

The responses observed were the principal stresses (σ_1) in the lateral load case and also in the radial load case. With the response values of the samples, the response surface was created in order to visualize the tendency of values. Note that the responses are qualitative values; the values of the stresses are not significant, since the simulation needs the air pressure presence. The maximum principal stress is located on the radius formed for the R parameter.

The response surface for both cases are shown in Figure 25. Avobe there is the response surface for the radial load case, and one can notice that this case presents a minimum when the parameter *R* is in low levels and the *S* in high levels. The green squares show the values of the response for the samples simulated (nine in total). Note that some of them are hidden below the surface. The surface is an interpolation between the sample points. The figure below is the response surface for the lateral load case. This becomes almost a flat surface, which means that the interaction between the parameters has not a significant effect on the response and the effects are lineal. The minimum is also located on the low levels of *R* parameter and high levels of *S* parameter.

The two surfaces are quite similar and both coincide with the fact that the minimum stresses are achieved when the R parameter is near the low limit and the S is in the high limit. In this case the two objectives minimize the first principal stress in each case, are achieved with the same configuration (same optimum). Taking into account this fact it is not necessary to find an optimum to minimize the objectives separately, which would require the application of a multi-objective optimization algorithm. For this reason, the sidewalls were configured as this optimum; the *R* parameter was fixed at 5 mm and the *S* at 7 mm.

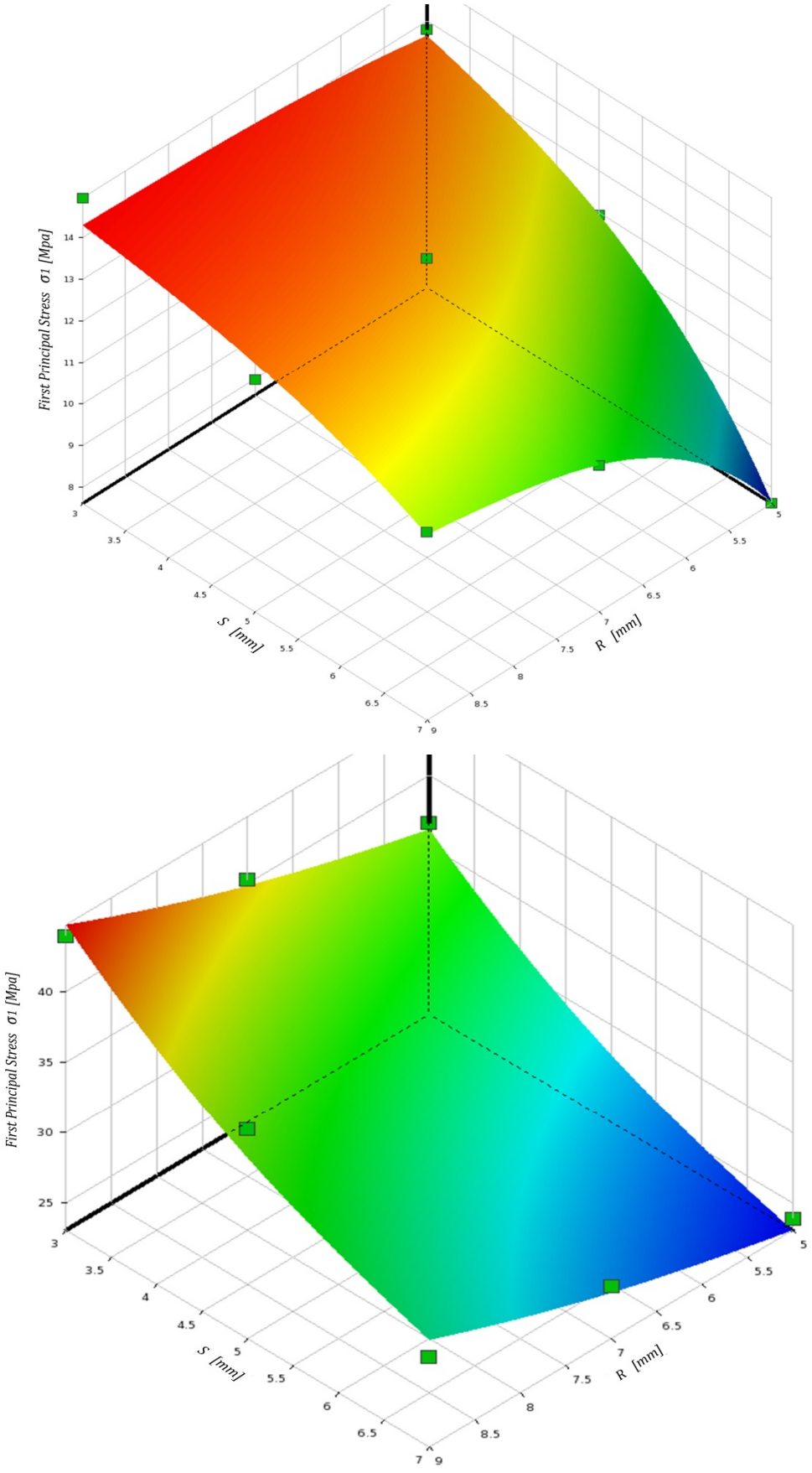

Figure 25. Response surfaces. In green squares, the response value for the samples tested. Above for the radial load case and below for the lateral load case.

5.1.4 Stresses determination

After the optimization of the contour and sidewalls, the dimensions for the rim had been defined. Then a simulation of half rim modelled with aluminium alloy was carried out. The three load cases were studied; radial, lateral and braking. All three with the air pressure applied. The value of principal stresses and its orientations were looked for. These would be crucial afterwards to orientate the fibres on the laminate.

Although the material and the thicknesses of the parts simulated were not the same as in the future carbon fibre piece, the simulation could give important information. The analogy between the aluminium alloy rim and the future carbon fibre's rim can be done because the stresses and its orientations do not depend on the material since they are imposed for the geometry and the boundary conditions, as external loads and constrains. The deformation is small and the geometry does not change in a non-linear way (that means that the stiffness matrix of the model (see section 3.3.3) remains constant during the deformation). One can conclude that the stresses do not change when the deformation changes the geometry. The deformation is actually the magnitude which depends on the material, because it is directly related with the material's elastic properties.

As usually in this thesis, the presentation of the results is separated between contour and sidewalls since they are different parts with different future laminate configurations.

Simulation results

The results obtained were the values of the principal stresses (σ_1, σ_2 and σ_3) and the direction for each one and shear stresses. The whole rim was modelled in order to visualise the real behaviour. The mesh of the model had an average skewness of 0,2071 which validate the mesh quality.

In order to visualize the principal directions (where the principal stresses are aligned), vector plots for principal stresses were a useful tool. This kind of graphics shows us with different arrows (one colour for each principal stress) in which directions are acting the principal stresses. This information will be essential afterwards when orienting the layers of the laminate.

- *Contour*

First of all, a coordinate system was defined for the contour in order to refer and orientate the stresses and afterwards the plies for the laminate. It was shown before on Figure 22.

In the three loading situations, the maximum first principal stresses are located approximately at the same place. Therefore a deeply study on the radial load case was done and generalized for the other load cases.

The results show that the maximum principal stress (σ_1) is located on the bottom of the rim, on the part of the contour in the tire side (see Figure 26). It can be understood as a consequence of the high pressure of the air inside the tire and the radial loads, which induce a bending moment on the contour.

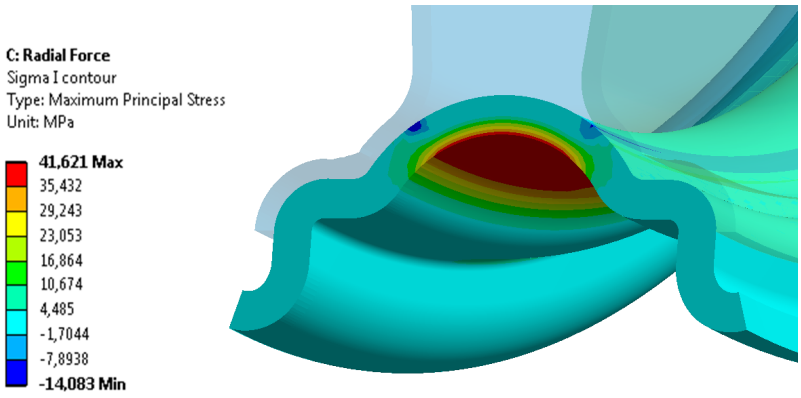

Figure 26. First principal stress acting on the contour for the radial load case. The maximum is located on the lower part of the rim.

It has been seen in Figure 26 that the critical point of the contour is located in the bottom of the rim, near where the loads are applied. The second principal stress was also found, and then it was possible to determine the plane stress state of the critical point in the contour. The first and second stresses are alienated with the X and Y axes of the contour's coordinate system (see Figure 27).

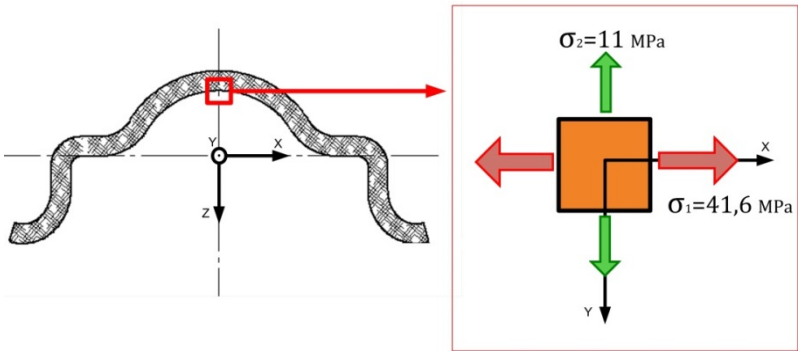

Figure 27. Plane stress's state on the critical point of the contour. Radial load case.

The analysis was completed by drawing the Mohr´s circles and finding the shear stresses in the plane. The illustration of the Mohr's circles (see section 3.1.6) is presented on the Figure 28. The red solid circle represents the plane stress's state on the plane formed for the first and second principal stresses (XY plane for the contour's coordinate system), which is the plane showed on Figure 27. With the Mohr's circle can be clearly seen that the highest shear stress acting on this plane is τ_{12}. However there is another high shear stress which is not located on this plane τ_{max}. This shear stress is located on the plane formed between the first and the third principal stressess (since it is located on the outer mohr circle between both). More specifically, this stress is oriented at 45 degrees between both principal stresses (first and third), which is the same that at 45 degrees between the X and Z axes.

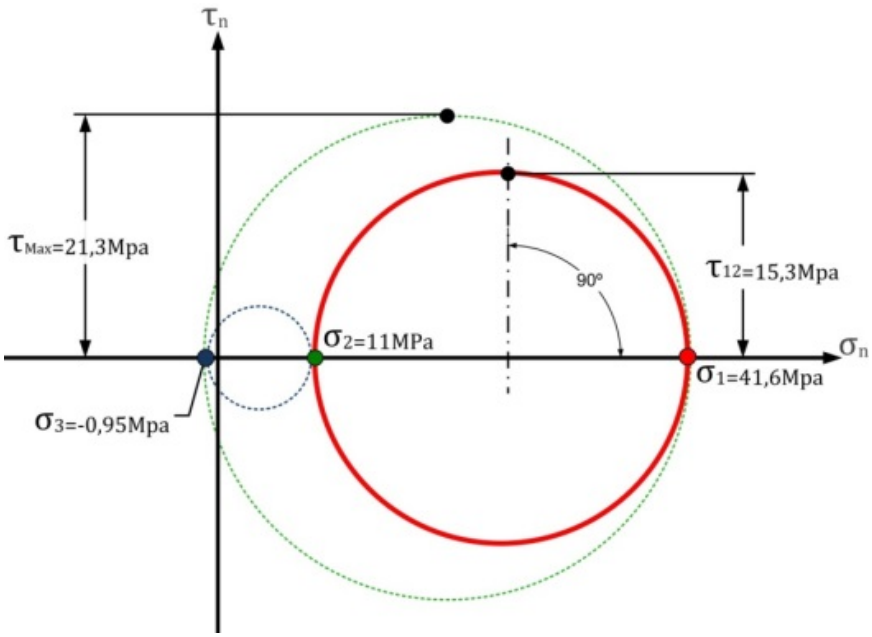

Figure 28. Mohr's circles of the stress state on the critical point on the contour in the radial load case. The solid red circle is the Mohr circle in the X-Y plane. On this plane the principal stresses acting are σ_1 and σ_2, with a maximum shear stress between both τ_{12}.

The other loading cases were also studied in the same manner and the stresses on the critical points were recollected and listed on the Table 9. The higher values were found at the lateral force case (σ_1 = 64,7 MPa and σ_2 = 19,6 MPa).

Table 9. Values of the principal stresses in the contour for the different loading cases.

Loading case	Principal stresses [MPa]		
	σ_1	σ_2	σ_3
Radial	41,6	11	-0,95
Lateral	64,7	19,6	-0,8
Braking	29,5	5,9	0,8

At this point one has to remember that rim is modelled in aluminium alloy and the thicknesses of the part are only estimations. Therefore the question is how much load the sidewalls save to the contour and if it is safe believing that the real sidewalls will pick the same load to the contour as they are doing in the simulations. The values were then compared with the ones obtained during the contour optimization (σ_1 = 86,7 MPa and σ_2 = 28,1 MPa), where the interaction with the sidewalls is not present. There is approximately 20 MPa of difference on the first principal stress. Note that in the optimization process, only the air pressure was applied, and the stresses are higher than in the lateral load case. Then it is reasonable to say that, in the contour, the influence of the air pressure is more significant than other loads.

Since the interaction with the sidewalls was not clear and in order to design the contour safely, it was considered not take into account the sidewalls for the contour design. The loads considered were then the ones found on the optimization of the contour: σ_1 = 86,7 MPa and σ_2 = 28,1 MPa.

Another thing that supports this decision was the mistrust against the bonding between the parts. In the simulation, it is an ideal bonding which can support any load without the separation of the parts, but in the reality the bonding phase has a limit that has also to be taken into account (it will be explained further on the assembly section).

- *Sidewalls*

For the sidewalls the three load cases were studied. First the radial load case was simulated. The radial load and also the air pressure induce compressive stresses on sidewalls that orient the third principal stress radially. Figure 29 (a) presents the vector plot for one sidewall (since the reaction is symmetric on both). The minimum value (the high compression) was located near the hub with a value of σ_3 = -35 MPa.

The lateral load case is the more asymmetric. It induces compressive stress on the sidewall where the lateral force is acting and tensile strength on the other one; this can be seen in Figure 29 (b). The minimum value for the third principal stress is also located near the hub, σ_3=-54 MPa.

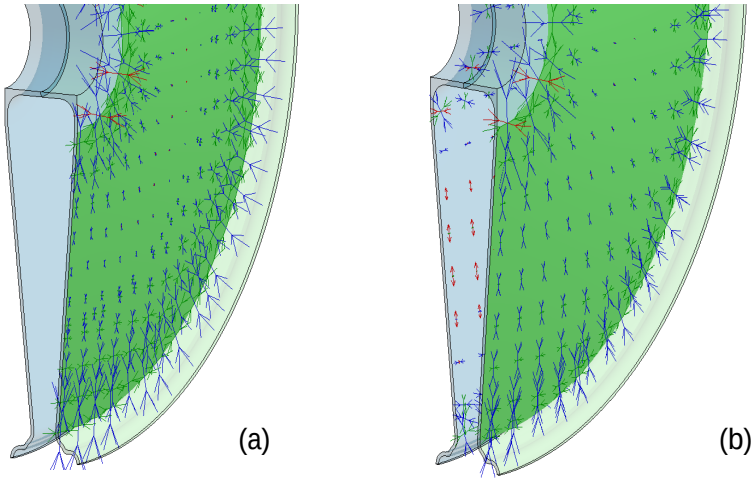

Figure 29. Vector plot of the principal stresses. (a) Radial load (b) Lateral load. In red, the first principal stress; in green, the second; and in blue, the third. The stresses are oriented mainly radially.

The braking case was also studied. This kind of load induces remarkable shear stresses near the hub. Figure 30 presents the results of the simulation. The maximum value observed is τ_{max}=19 MPa. This maximum can be clearly seen as a red circle on the figure near the hub. It is caused due to the fact that the hub is totally constrained (fixed) and the torque on the rim is transmitted with the shear stress through the sidewalls. It can be considered afterwards to place some extra reinforcement on the hub zone.

Having analysed the three cases one can conclude that the stresses are mainly radial in the lateral and radial load cases. In the brake case, the load induces a shear stress which achieves a maximum near the hub. In the sidewalls' coordinate system (already defined in Figure 24), the stresses considered for the next steps on the design process are:

- σ_x=-54 MPa
- τ_{xy}=19 MPa

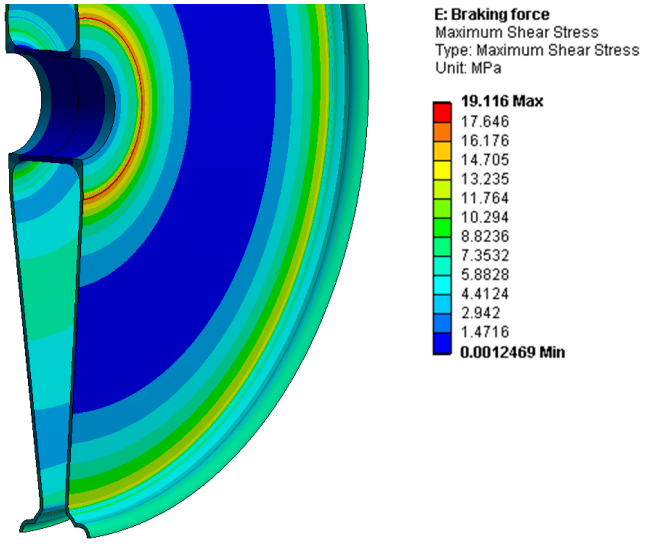

Figure 30. Shear stress for the braking load case. Due to the torque induced for the braking, the highest shear stresses are transmitted to the hub zone.

5.1.5 Laminate configuration

The laminate determination is a crucial part when designing with composite materials. The previous sections in this chapter provide us the necessary information to size properly the laminate.

The composite material chosen was carbon fibre with epoxy that as it was explained on the theoretical framework. It combines a lightweight while maintaining excellent mechanical properties. Therefore is an excellent choice for this kind of applications.

Before starting the laminate's design some assumptions will be taken into account:

- Laminates with mid-plane symmetry are desirable.
- A minimum number of plies is desirable to be placed at the four main orientations (0°, 90°, 45°,-45°), or other ones (see section 3.2.7).
- All the laminates are assumed as thin laminates that can be studied at each point as a plate (plane stress).
- The properties for the plies contemplated will be the ones presented on the theories. Since there is a big variety of suppliers and types, this is considered a good estimation. The design will be checked afterwards with the properties of the plies purchased.

In order to configure the laminate one has to know the proportion of the fibres which must be oriented along the different directions. For this purpose, there are tables that help determine the proportions in which the fibres should be placed, considering the efforts that will be applied to the laminate. The tables take into account the Tsai-Hill failure criterion and give accordingly the optimum compositions for the laminate. In this thesis the ones used are presented by D.Gay and S.V.Hoa on [12].

- Contour laminate

The contour has maximum tensile and compressive stresses occurring on the axial direction (the *X* direction of the contour's coordinate system). The first principal stress is oriented in this

direction. Then a good configuration of the laminate for the contour has to contain a high proportion of the fibres aligned along this direction.

The stresses found for this part were: $\sigma_1 = \sigma_x = 86{,}7$ MPa and $\sigma_2 = \sigma_y = 28{,}1$ MPa.

Then the proportions of stress to introduce on the table are:

$$\overline{\sigma_x} = \frac{\sigma_x}{\sigma_x + \sigma_y} = \frac{86{,}7\ MPa}{114{,}8\ MPa} = 0{,}755 \approx 0{,}75$$

$$\overline{\sigma_y} = \frac{\sigma_y}{\sigma_x + \sigma_y} = \frac{28{,}1\ MPa}{114{,}8\ MPa} = 0{,}245 \approx 0{,}25$$

With the stress proportions at each orientation defined, it was possible to determine the desirable fibre's orientations. The Table 12, in the appendix B, is used when the both stresses (*x* and *y*) are tensile stresses. In this table the stresses are in a stress resultant form (N_x and N_y); the stresses are multiplied for the laminate's thickness. Nevertheless the proportions are the same (because the thickness is multiplying all the stresses) and the table can be used as normally if one understand the proportion for σ_x as N_x and the one for σ_y as N_y.

Since there is not a determined configuration for the stresses proportions found before, an approximation between the three nearest configurations is done. The final fibre proportions for the contour laminate, with the contour's coordinate system are shown on the Figure 31 below.

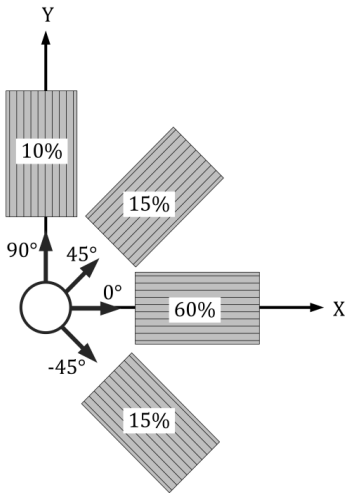

Figure 31. Fibre proportions for the contour. The fibres are placed mainly on the x direction due to the high first principal stresses acting there. Nevertheless other orientations are also reinforced.

The proportions were defined then the laminate could be determined. For deciding the final laminate layout some aspects should be taken into account:

- Due to the bending moment a tensile and compressive stresses are induced on the inside and outside parts of the contour. This phenomenon was seen on the stress determination section. The distribution of the stresses due to the bending moment is illustrated on Figure 32, note that the highest values are located at the external parts of the contour. Therefore it is appropriate to orientate the outer plies on the *X*

orientation (axial orientation) to withstand these high stresses (tensile and compressive ones).

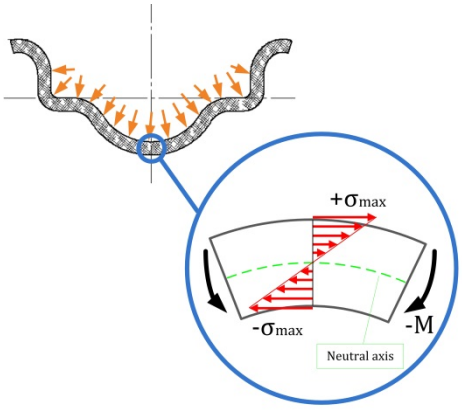

Figure 32. Bending moment acting on the contour and stress distribution that it causes. In green, the neutral axis where the stresses are zero.

- The maximum first and second principal stresses are located on the outer part of the contour; therefore there exists also a high shear stress (τ_{12}) between them on their plane (see the Mohr's circles at Figure 28). Then it is advisable to intersperse a ply with the fibres oriented to ±45 degrees.

- The contour has a very small radius (*R2*) (Figure 16 for the sketch), therefore it is recommendable to situate a woven fabric on the top of the laminate since it is easier for those to cover small radius (more curvature is allowed compared with unidirectional layers).

- In order to accomplish the tolerances for the contour (see Table 6 for specifications) the deformations should be small. Then the unidirectional layers are recommendable since they have better strength properties.

With these guidelines it was thought to place a group of unidirectional plies on the middle of the laminate to give enough strength and avoid an excessive deformation. Some woven fabrics were placed on the top, oriented on the axial direction (0°/90°), in order to do the manufacturing process easier (since it is easier cover curved surfaces) and to give integrity to the entire laminate.

The final laminate layup consisted in 20 plies, ten unidirectional layers and ten woven balanced fabrics. They were placed symmetrically ensuing with the fibre orientation's proportion found before and the guidelines assumed. In a compact form (see *Layup notation* in 3.2.7) the representation of the final laminate configuration is:

$$(0\,F_2 / 45\,F_2 / 0_3 / 45\,F / 0_2)_S \quad .$$

The Table 10 below shows with more detail the laminate configuration.

Table 10. Final configuration for the contour's laminate.

Number of Ply	Constituent	Orientation	Thickness [mm/ply]
1, 2	Woven fabric	0°/90°	0,22
3, 4	Woven fabric	45°/-45°	0,22
5-7	Unidirectional	0°	0,15
8	Woven fabric	45°/-45°	0,22
9, 10	Unidirectional	0°	0,15
---------- Mid-plane symmetry ----------			
11, 12	Unidirectional	0°	0,15
13	Woven fabric	45°/-45°	0,22
14-16	Unidirectional	0°	0,15
17, 18	Woven fabric	45°/-45°	0,22
19, 20	Woven fabric	0°/90°	0,22

The thickness for the laminate was estimated, for the unidirectional layers in 0,15 mm and for the woven fabrics in 0,22 mm [8]. Therefore the thickness estimated for the contour is 3,7 mm.

- Sidewalls laminate

The sizing for the sidewall's laminate follows the same design process as in the contour. First of all the stress proportions were calculated in order to know the proportions of fibres at each orientation.

As it was seen on the stress determination for the sidewalls, the zone near the hub is under higher stresses than the rest of the part, specially the stresses induced during the braking. Accordingly, it was thought to strengthen this part. The laminate would be the same along all the sidewall but with some more plies on the hub zone in order to acquire a plus of safety.

First the stress's proportions will be calculated, remember that the *X* orientation on the sidewall's coordinate system is the radial orientation. On one hand, near the hub the stress distribution is σ_x=-54 MPa and τ_{xy}=19 MPa, the stress proportion is approximately (taking absolute values):

$$\overline{\sigma_x} = \frac{\sigma_x}{\sigma_x + \tau_{xy}} = \frac{54\,MPa}{73\,MPa} = 0{,}739 \approx 0{,}70 \quad ,$$

$$\overline{\tau_{xy}} = 1 - \overline{\sigma_x} = 0{,}3 \quad .$$

The optimum composition can be found on the Table 13 in the appendix B. For this laminate the fibre proportions are shown on Figure 33 (a).

On the peripheral zone the stress proportion were estimated as almost all radial since the shear stresses are not as high as in the contour:

$$\overline{\sigma_x} = 0{,}9 \quad ,$$

$$\overline{\tau_{xy}} = 0{,}1 \quad .$$

[8] Source: www.hexcel.com

The optimum composition would be a bit different. It is presented on the Figure 33 (b). This configuration is also found one Table 13.

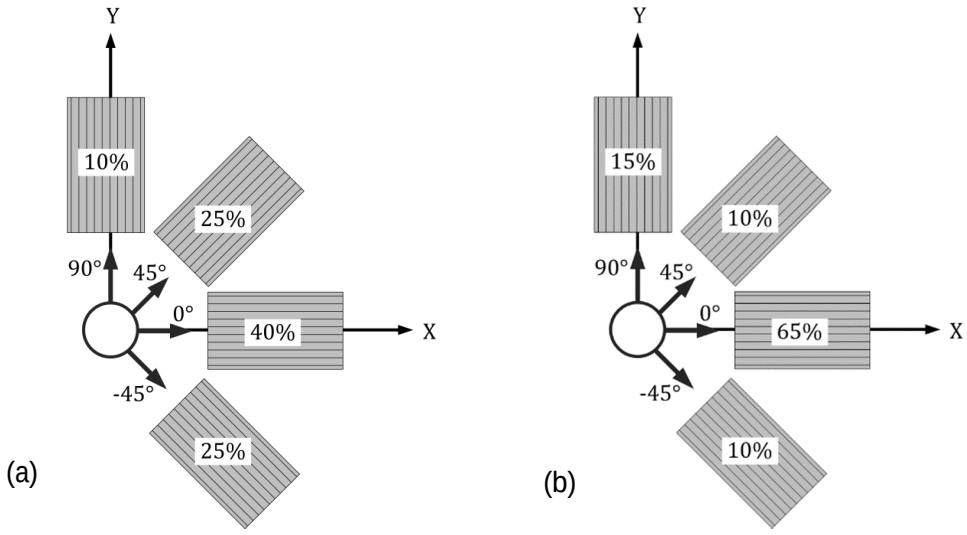

Figure 33. Fibre proportions for the sidewall. (a) Near the hub, with more shear stresses the proportions are more shared. (b) Peripheral zone, the principal amount of fibres is placed on the radial orientation (x direction).

Notice that at minimum a ten percent of the fibres are placed at each orientation as a safety step (see *Ply orientation* at 3.2.6).

When these two fibre proportions were defined, the laminate configuration could be studied. Some points were taken into account before that:

- Since the sector of the rim touching the ground is constantly changing it was though appropriate to divide the sidewall in different laminate sectors to orientate the fibres better. This was done by dividing the 360 degrees of the sidewall by 18 sectors of 20 degrees each as it was considered for the loads application.

- Only the unidirectional layers will be cut into sectors. In order to provide more integrity on the laminate the fabrics will not be cut. The fabrics are more isotropic then the orientation on the sectors is not as important as it is for the unidirectional plies.

Finally laminates for the sidewalls was configured as:

Peripheral zone: two unidirectional plies at zero degrees (radial orientation) and one fabric between them (not cut in sectors).

Near hub zone: The plies on the peripheral zone continue on the hub zone and two extra fabrics are placed between the plies.

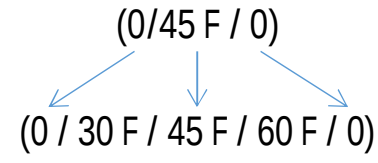

The unidirectional layers are cut and placed for each sector separately; the fabrics are placed just in one piece to give more integrity to the laminate. The two extra plies on the hub zone give a reinforcement which will help to support better the braking load.

5.2 Design validation

In order to validate the design, a simplified model of the rim was simulated with ANSYS® ACP (ANSYS Composite PrePost). This component gives us the possibility to simulate the model more accurately since it allows layered models with the anisotropic properties characteristics from composite materials. For the validation of the design, the model was split in contour and sidewalls.

5.2.1 Contour validation

The validation of the contour was done through simulating a two degrees sector with the layered configuration decided before. The air pressure was applied as a boundary condition. It was simulated as a shell with thickness with the element type SHELL181 which allows the layered model from the ACP component.

In order to introduce correctly the model to the ACP pre component, some variables had to be defined. First of all the contour's coordinate system was defined and then the zero degree axis in order to orientate the plies afterwards. The software needs this information to understand properly the configuration of the laminate.

The materials used were also defined. Two types of layers are chosen for create the laminate, unidirectional plies and plain wave woven fabrics. Both were defined on the theoretical framework. One can easily see the differences between the unidirectional layers and woven fabrics with the polar representations of their elastic properties, on the appendix C. The unidirectional plies are highly anisotropic (see Figure 46) but also stronger on the fibre direction. Otherwise the woven fabrics are more isotropic and stable (see Figure 47), but with less strength.

When all the plies were defined, the simulation was launched. The results were analysed with the ACP post component. For the validation of the design the main results analysed were the deformations and the reserve factor for Tsai-Hill.

First the deformations were checked. The Figure 34 shows the results for the deformations in the axial direction (*X* axis) with sign (positive if they are oriented on the positive *X* axis direction). The values are reasonable and remain below the tenth of a millimetre on the side where the tire is held.

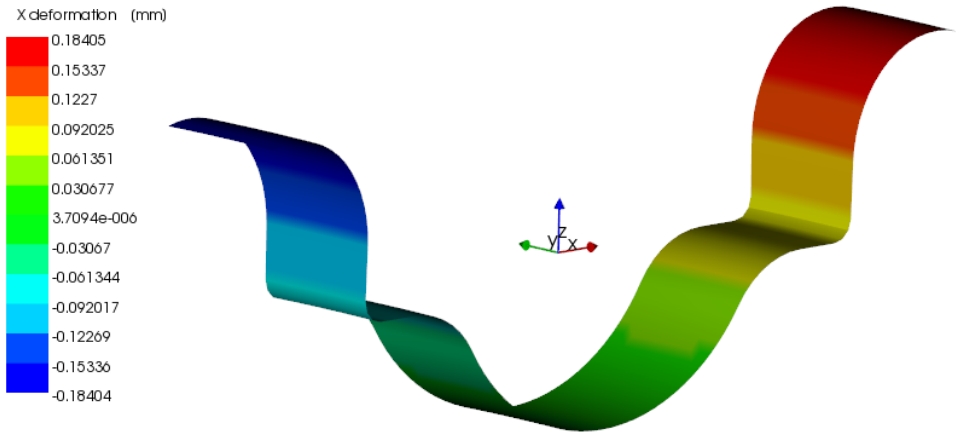

Figure 34. Deformation on the X axis of the contour.

On the other hand, revising the failure criterion the results are also satisfactory. Reviewing the reserve factors for the Tsai-Hill criterion in 3D form, the minimum value is located on the middle of the contour with a reserve factor of 1,67. The Figure 35 shows the ranks for the failure criterion and its locations on the contour.

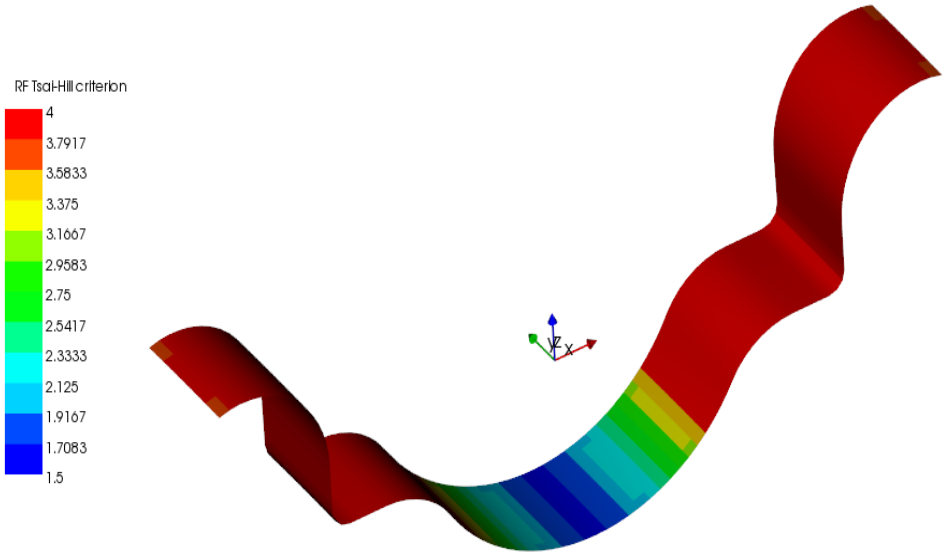

Figure 35. Reserve factor on the contour for the Tsai-Hill criterion

A deeply study was done on the critical point (the middle of the contour), looking at the failure criterion at each ply. The Figure 36 present the reserve factors for each ply and allow us to know which ones are the most critical.

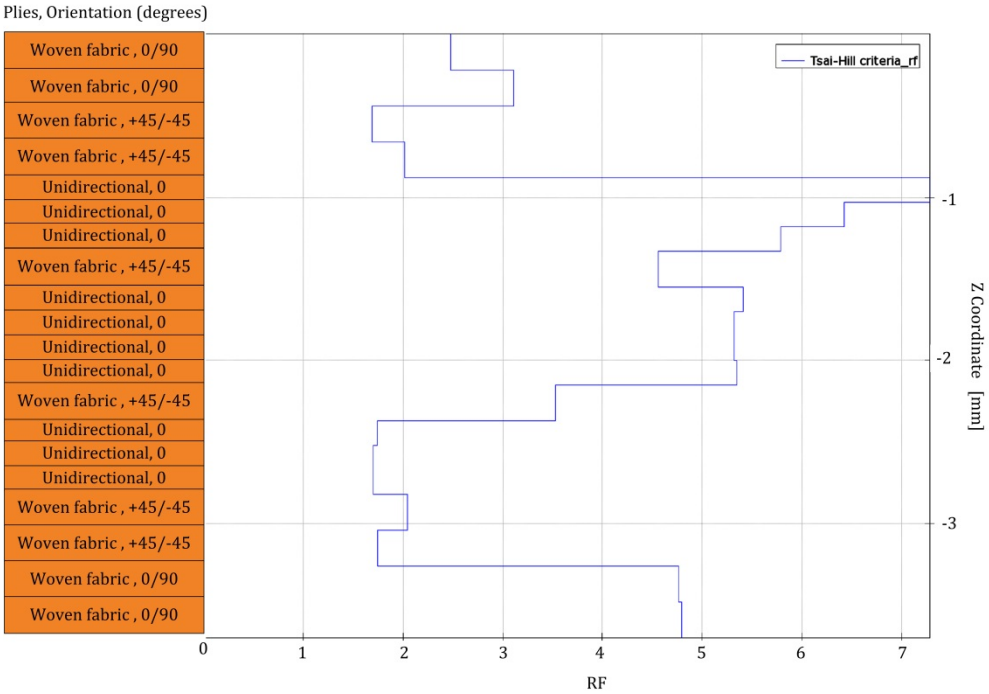

Figure 36. Reserve factor for the Tsai-Hill criterion (3D) for each ply, with layer type and orientation specified.

Note that the failure criterion is used in its 3D form, then it also take into account interlaminar stresses. The distribution is asymmetrical and depending on the orientation of the plies the values are different since they are supporting different types of stresses. The plies near the neutral axis (see Figure 32) have higher reserve factors since the value of the stresses are lower there.

It is also interesting to look at the same study using the failure criterion in the 2D form, which only considers the stresses occurring on the ply. Figure 37 shows the results, in this case the minimum reserve factor is 3,19 and it is placed on the lower ply due to the compressive stress. Here is more evident the bending's distribution of the stresses, the plies on the neutral axis have significantly higher values for the reserve factor.

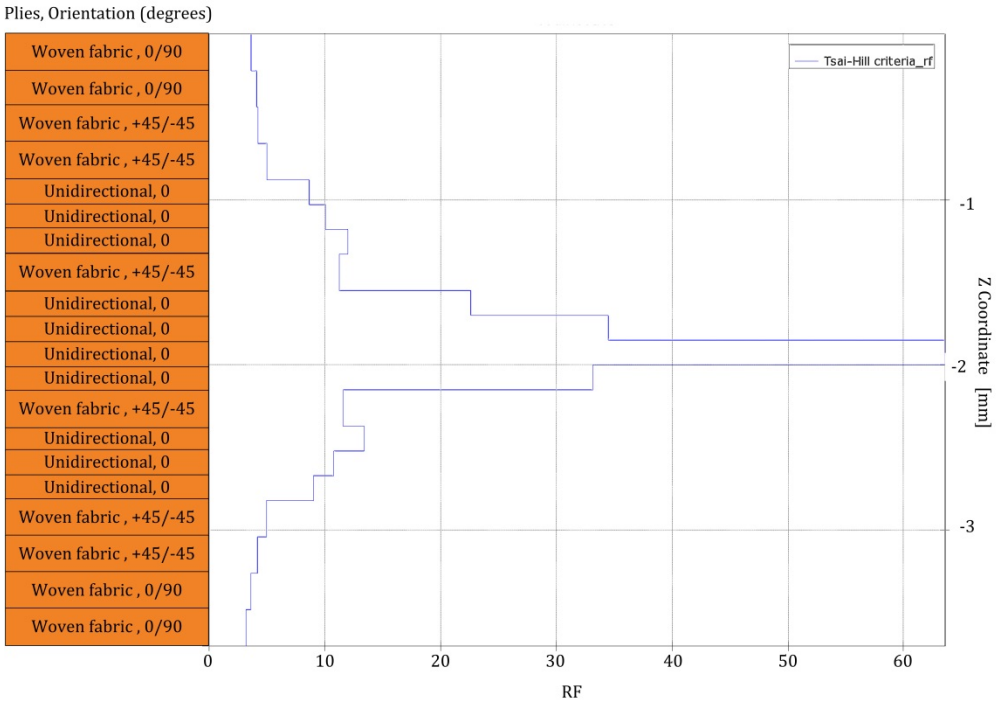

Figure 37. Reserve factor for the Tsai-Hill criterion (2D) for each ply, with layer type and orientation specified. On the neutral axis the reserve factors are the highest ones since the stresses are almost zero.

The contour becomes validated since the deformation and the reserve factor for the failure criterion are found within a range of acceptable values. One cannot forget that the design wants to be on the limit where the safety and the best performance are achieved, then a reserve factor of 1,67 is an almost optimum value. The deformation has an order of magnitude of a tenth of millimetre on the tire support zone, it also validates the contour.

Since the contour is sized without taking into account the help that the sidewalls provide, it could be possible to take off some ply while maintaining a good reserve factor, but then the deformation would be also higher.

5.2.2 Sidewalls validations

For the sidewall validation, the geometry was simplified by splitting the rim along its symmetry plane, therefore only one sidewall was simulated. The contour was also modelled in order to achieve the right boundary conditions.

Then model was divided into sectors in order to place the laminate properly, those were radial sectors and also the central circumference near the hub where some reinforcements would be placed. The Figure 38 shows half model, and the different sectors and the coordinate system for each sector.

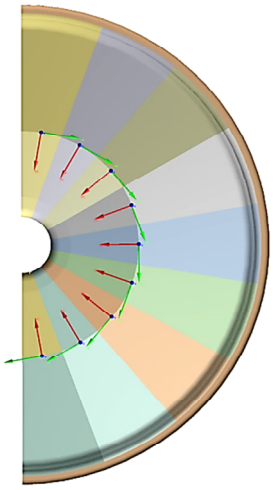

Figure 38. Half modelled rim. Divided into nine radial sectors and one circular on the middle. Each sector has its coordinate system. In red, X axis, in green Y axis.

As well as in the contour's validation, the laminate was introduced to the ANSYS® ACP Pre component specifying the plies and the orientations of these ones accordingly with the design specifications. In order to study the function of the reinforcement placed on the centre, the loads applied were the brake force and the radial load. As in the contour's validation, the points to review carefully are the reserve factors for Tsai-Hill criterion and the deformations, as the possible grade of buckling of the sidewall.

First the shear stress was checked to see if the simulation had been well defined. Nevertheless the deflection of the rim due to this load is very acceptable; the Figure 39 shows us the deformation on the Z direction of the global coordinate system. The deformation is about the tenth of millimetre, a quite good value.

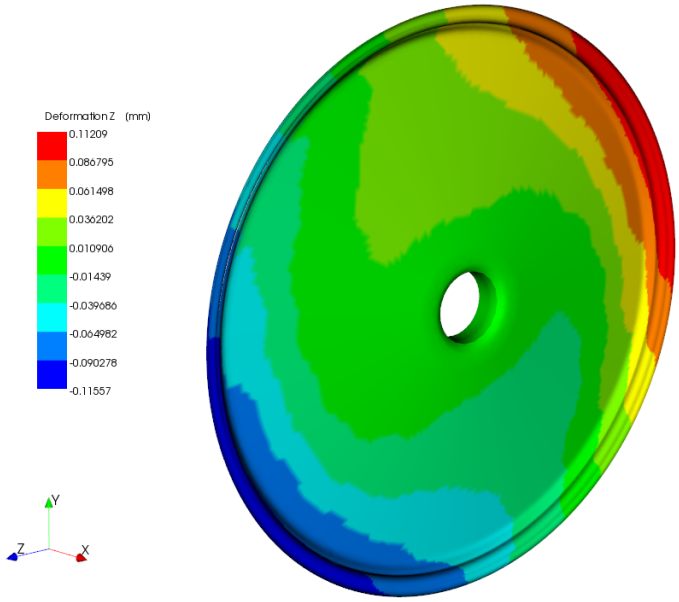

Figure 39. Deformation due to the brake load (in the global axis Z orientation).

It was also important to check the buckling tendency of the rim. It is apparent if one looks at Figure 40, which shows the sum of the displacements (x,y, and z). Due mainly to the air pressure on the tire and the radial load, the sidewalls tends to bend. If we analyse the results of this figure, the central part of the rim is well held for the contact with the hub and the peripheral zone for the contact with the contour. Then the weakest part is on the middle part between both contacts, as one can see with deformations that reach 0,44 mm, definitely a safe result.

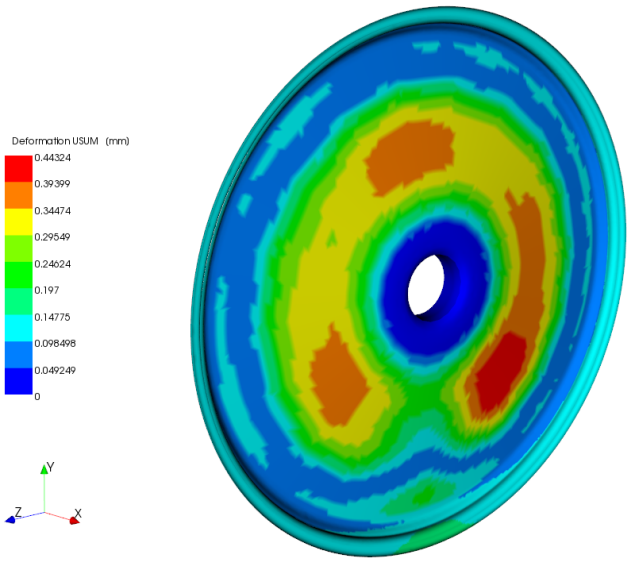

Figure 40. Sum of deformations USUM on the sidewalls with a radial load. In red the highest values shows the tendency of the sidewall to buckling.

Once the deformations were accepted as safe, the safety factors for the failure criteria were reviewed. The Figure 41 presents the results of the reserve factor for the Tsai-Hill criterion in the three-dimensional form (the minimum reserve factor of a ply at each point of the rim, since the failure criterion is applicable at one point). The minimum reserve factors are located near the hub and near the contour respectively. At the bottom of the sidewall there are some points with a reserve factor oscillating between 1,5 and 2. Near the hub the values are around 3 with some point with a lower reserve factor around 2.

For the Tsai-Hill 2D criterion (which only takes into account the stresses on the ply) the values are too much high.

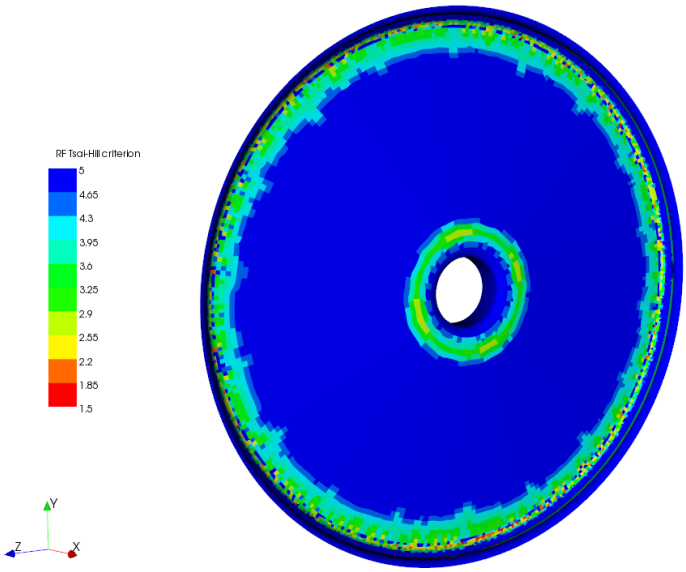

Figure 41. Reserve factor for the Tsai-Hill criterion.

With these results the sidewalls were validated and the design process could keep going without having to resize the parts.

5.2.3 Weight reduction

The present thesis has presented a possible design for the rims that it has been validated. The materials considered during the design process have average properties which provide a trustworthy estimation on the material, but the weight of it is difficult to estimate properly. Concerning to this application of the design, few grams of variation can be significant.

In order to provide an estimation on the weight of the parts, a real material is selected. The unidirectional and woven fabrics are made of the same type of fibre [9] ; a high strength carbon fibre. The thickness considered for the layers is a guideline for selecting a possible option: the unidirectional ply selected [10] has an areal weight of 160 g/m2 and for the plain-wave woven fabric [11] an areal weight of 193g/m2.

The weight reduction is presented below but the reader must notice that this is only an estimation. Due to the manufacturing process, material selection and other factors the final weight can vary significantly from the weight presented here, then the weight reduction must be considered carefully. The weight of the current contour is 450 g and the weight for the spokes is 244 g (the weight of the hub is not considered since it will be neither considered for the carbon fibre rim). The weight calculations for the designed rim are:

Contour:

Area: 0,08618 m^2. *Configuration:* 10 unidirectional and 10 woven fabrics.

Weight of the layers = 0,08618 m^2 x (10 plies x 160 g/m^2 + 10 plies x 193 g/m^2) = 304g

Estimated laminate's weight = 304g / 0,80 [12] = 380 g

Sidewalls :

Total area: 0,14204 m^2 . *Configuration:* 2 unidirectional plies (in sectors) and 1 woven fabric.

Reinforcement area: 0,032070 m^2 *Configuration*: 2 woven fabric

Carbon fibre layers weight = 0,14204m^2 x (2 plies x 160 g/m^2 + 1 ply x 193 g/m^2) + 0,03207m^2 x (2 plies x 193 g/m^2) = 85 g x 2 sidewalls = 170 g

Estimated laminate weight = 170 g / 0,80 [12] = 212 g

Table 11. Estimated weight reduction for the designed rim regarding the current rim weight.

	Contour	Sidewalls / spokes	Rim (without hub)
Current rim	450 g	244 g	694 g
Designed rim	380 g	212 g	592 g
Weight reduction	70 g (15,5%)	32 g (13,1%)	102 g (16,9%)

[9] Torayca® T300B 3K 40B C2

[10] HexForce® G0827 6 1040 TC PV

[11] HexForce® G0814 6 1000 TCT

[12] Estimated weight fraction between carbon fibre and epoxy resin. It will vary depending on the manufacturing process.

Finally the estimation for the rim's weight is 592 grams, which is a reduction of 102 grams from the current aluminium rims, almost a 17% of reduction. This reduction is calculated without taking into account the hub. In Table 11 the weight reduction is separated into contour and sidewalls. The biggest reduction is achieved on the contour, where a reduction of 15,5% is achieved. The sidewalls has less weight reduction since the aluminium spokes used currently are quite lightweight, and the sidewalls has a big area which obviously increases the weight.

5.3 Assembly

Until now it has been studied and designed the different parts of the rim separately, on one side the contour and on the other, the sidewalls. This section, therefore, intends to explain how the different parts interact with each other to form the rim, including a brief study of the design of the hub and the contact between it and the sidewalls.

The premise is also to incorporate the design of the rim as much as possible with the work done before for the HiGtech team, respecting the elements that are already designed. This is the case of the shaft which is dimensioned with a diameter of fifteen millimetres, the bearings that are already selected [13] and all the brake system which use an ISO standard 6-bolt brake disc.

The joints between the parts would be glued. This type of joining consists in the molecular attraction between the two parts to be bonded and the adhesive which has to be able to transfer the loads properly. Some of its advantages are that the distribution of the stresses is done usually over an important surface and that it is a lightweight mode of joining.

When designing bonded joints one should keep in mind few things in order to design a good union [35]:

- The glue should not resist tensile stresses
- The union should work supporting shear stress on its plane
- Possible thermal dilatations

There are many types of adhesives for composites materials, the ones more used could be epoxies, polyesters, polyurethanes and methacrylates. In this thesis it is going to be use an adhesive based on epoxy resin, as could be Araldite®, since it is appropriated with the materials used.

The shear strength reference values for Araldite® considered are at 20°C [35]:

- For cold bonding (without curing process): $\tau_{rupture}$=10 MPa
- For hot bonding (curing between 120°C and 180°C): $\tau_{rupture}$=17 MPa

The adhesive thicknesses are usually between 0,1 and 0,3 mm.

5.3.1 Joints

Sidewalls with the hub

The hub should be designed especially for this rim since the contact with the sidewalls is a crucial part of the assembly. Here is presented an approximation to the final design, giving some guidelines. In order to avoid stress concentrations the low sidewall corners are rounded,

[13] SKF® E2.6202-2Z/C3 from the branch of energy efficient bearings (E2) of SKF®.

as well as the contact where it fits on the hub. It is also a way of increasing the contact zone for a safer bonding. The Figure 42 shows in pink the bonding phase between the hub and the sidewalls in a section view of the assembly.

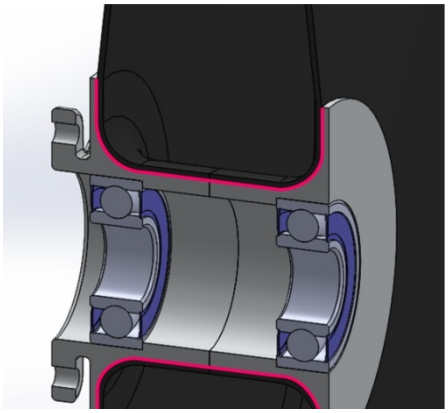

Figure 42. Adhesive bonding with the hub. (Section view) In pink, the adhesive phase.

Contour with sidewalls

Between the contour and the sidewalls the same adhesive bonding is used. The surface is much bigger than in the hub then it is a safer contact (see Figure 43). It would be a good option since the distribution of the loads will be around all the sidewalls.

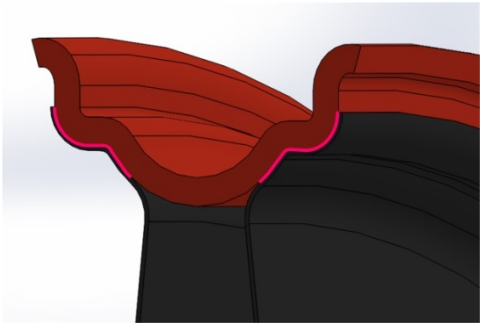

Figure 43. Adhesive bonding between the contour and the sidewalls. (Section view) In pink, the adhesive phase.

The hub is divided into two parts in order to make possible the mounting of the whole assembly. The Figure 44 shows an exploded view of the assembly.

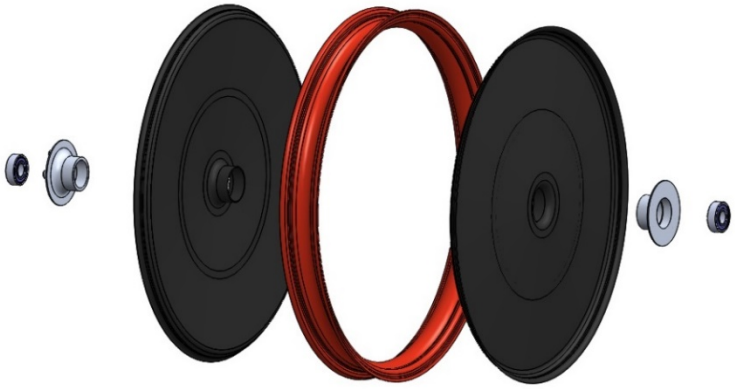

Figure 44. Exploded view of the assembly. The two sidewalls in black, and the contour in red. The hub is divided into two parts in order to mount the assembly, the bearings are also represented.

5.4 Manufacturing process

A brief guideline for the manufacturing process of the parts will be described in this section. It is true that there are a few different methods to fabricate the new designed rim, but here it is going to be presented which is thought to be the cheapest and easier one.

- Sidewalls:

The sidewalls can be manufactured using a vacuum bag moulding process. This process starts placing the layers impregnated with the resin over an open mould which has the desired shape. Then the part is sealed hermetically with a flexible film forming a bag. The vacuum is made inside the bag with a vacuum pump and the atmospheric pressure outside compress the film and the composite layers to form the final part. Then one has to wait a curing time for the hardening of the resin before take the part out of the mould, in ambient temperature can be a day long. This polymerization time (curing) will depend on the technical specifications for the epoxy used and also the ambient conditions as the temperature. This process can be improved with the application of heat or pressure. There are special ovens and autoclaves[14] that are used for achieve high performance composites.

The Figure 45 shows schematically this method [36].

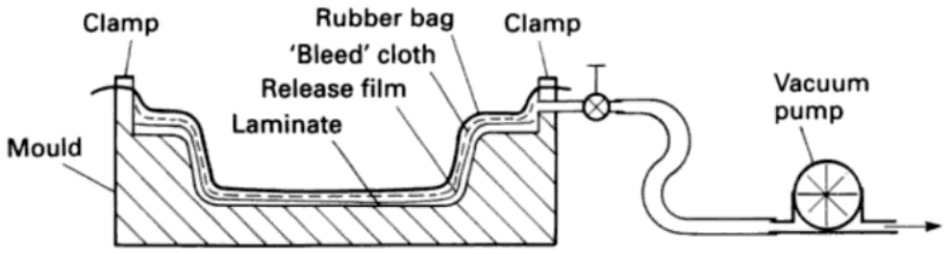

Figure 45. Vacuum moulding schematic. The laminate is pressed due to the atmospheric pressure, a vacuum pump takes the air inside the bag out.

The mould for the sidewalls can be made of metal as aluminium or also with cured epoxy. The mould should be machined with a numerical control milling or lathe (with spinning the mould) due to the curved surfaces of the sidewall.

With a heat curing process it is desirable to not use a metal mould since the usual big thermal expansion of the metal can vary the dimensions of it.

- Contour

For the contour, the process is different since the mould has to be divided into few parts for allow the unmould process. The process explained is based on [12].

First a positive epoxy or silicon mould is cut using a special tool with the contour profile. It can be done mounting the special tool on a lathe and turning the epoxy mould. Then with a pre-preg carbon fibre layers the negative mould is manufactured using the first mould, but this time the negative mould is divided into three parts to make easier the unmoulding operation.

[14] Autoclaves are pressure vessels which can control the pressure and the temperature inside. They are used for the curing processes in high performance composites as for the aerospace and aircraft industries.

There are two ways to proceed at this point, one is to divide the positive mould (the first one) and do a compressive moulding process, placing the laminate between the positive and the negative mould. Another way is to do vacuum moulding with the negative mould obtained.

6 Discussion and conclusions

The overall aim of this thesis was to design a rim for a fuel efficient competition vehicle made of carbon fibre reinforced polymer and, at the same time, advance in understanding of composite material. The specific objectives were to design the rim safely and lightweight, compared to the current aluminium rims.

This chapter will summarize the findings of the thesis in relation with the design functionality and weight reduction achieved and will offer conclusions based on these findings. Future work will be recommended as well as some guidelines for projects that can be based on this one. In the end the some limitations encountered during the realization of the thesis are explained as well as a brief self-reflection.

- Design functionality

The separation of the rim between contour and sidewalls is considered an appropriate design way. It allows to control the laminate thickness of each part separately and orientate the layers in a better way. In addition, the contour gains integrity if it is made on one part, which is important for withstand the air pressure on the tire. The obtained estimated thicknesses are quite different, 3,7 mm for the contour and for the sidewalls 0,56 mm on the peripheral zone and 0,92 mm on the hub zone.

According to the results obtained with the finite element analyses of the laminate, the final design obtains reserve factors of 1,67 for the contour and around 1,5 for the sidewalls which is a good margin of safety. One has to remember that every part of a fuel efficient vehicle seeks to be as light as possible and the best performance is achieved with the minimum oversizing possible, which means design the parts with just the minimum necessary safety.

Regarding the contour, it was sized without considering the contact with the sidewalls since the 'help' that the sidewalls provide to the contour was not clear. Nevertheless, with a reserve factor of 1,67 the contour is considered safe enough. The deformations show a displacement of less than a tenth of a millimetre on the contact zone between the contour and the tire. This value is below the limit specified as a requirement and validates the design as well.

When taking a better look at the contact between contour and sidewalls the interaction between them could be understood better. After this the optimization on the contour could be analysed in order to know if some layers of the laminate could be taken off. If this option is followed the deformations and the reserve factors must be rechecked in order to validate the design again. The contour is a crucial part on the rim due to the high air pressure on the tire where a little bit of oversizing can be accepted.

The sidewalls have the minimum values of the reserve factor on the bottom of the rim, where the loads are applied. These value are between 1,5 and 2 depending on the point. When these values appears, when cornering, the wheel is always spinning and the points touching the ground are changing constantly, only loaded momentarily. For this reason these values of the reserve factor are tolerable and thus accepted. The reinforcement placed on the middle of the sidewall works quite well; it reduces the reserve factors on the zone near the hub and does not increase the weight on the peripheral zone, where the reinforcement is not needed. The tendency to the buckling of the sidewall due to the air pressure on the tire and the radial loads

was also checked and the results show a maximum deformation of 0,44 mm which can be clearly accepted as safe.

In conclusion the sidewalls are considered to work quite well and their shape makes the manufacturing process easier. The reinforcement on the middle is a good solution to withstand the stresses on the hub's zone better and not increase the thickness of all the laminate. On the other hand the sectorial disposition of the unidirectional layers have also good advantages supporting the radial load, since they have the same function of multiple woven fabrics crossed but with less weight and less thickness.

- Weight reduction

The weight reduction appears to be a difficult parameter to calculate during the designing phase. The generic materials considered during the thesis are in the end assimilated at real products which its aerial weight is used to calculate the weight of the rim. The sidewalls plus the contour are estimated to have a weight of 592 grams which represents a reduction of almost 17% in relation to the current aluminium rims. Nevertheless, this weight reduction has to be considered carefully since many factors are involved on the final rim's weight, including the manufacturing process and the final material selection.

The contour achieves a reduction of 15,5% of the weight in relation with the actual aluminium contour and the sidewalls a 13,1% in relation the weight of the spokes used currently. The weight reduction could seem small but the actual rims used for the team are actually quite lightweight. With an optimization on the contour the percentage could be higher. Nevertheless in competition level few less grams are well received.

- Future work and recommendations

The thesis has provided theoretical baggage in relation with structural parts made of composite materials, particularly with carbon fibre reinforced polymers. In other parts of the HiGtech team's vehicle a weight reduction can also be achieved using composites, a good option would be the chassis of the vehicle. Before that some more experience is needed and the manufacturing of the rims could be an appropriate start.

In relation with the rims designed in this thesis, few points should be reviewed before the fabrication of these. On one hand the manufacturing process must be studied further. The type of epoxy used and the curing conditions have to be known. The tooling needed for the manufacturing process has to be custom for the rim, which is basically the moulds and some tools for the assembly process. If the budget and the time allow it, building a first prototype for the rim would be a good option. It would provide experience on the manufacturing process and also a verification of the design, as well the real weight reduction. On the other hand the hub's design needs to fit into the whole design. The current aluminium hub could be optimised to reduce its weight or otherwise the design of the hub made of carbon fibre reinforced polymer could be studied since it can provide a better overall weight reduction for the rims. For this last option, the present thesis can provide useful information.

- Limitations and self-reflection

Some problems have been encountered during the realization of the thesis. The first one, at the beginning, was the evident lack of experience with the material used. It influenced somehow on the work with delaying the start of the design process. The lack of time was also another important factor.

However the realization of the thesis has been a great learning process where it has been acquired an overview and an understanding of the composite material characteristics, as well as more practice in finite element analysis. On this field, the first contact with the simulation of composite materials using ANSYS®ACP it has been also such a new experience.

7 References

[1] *What is the EU doing about the climate change? [Online]*
Available at: ec.europa.eu/clima/policies/brief/eu [Accessed 20/05/2014]

[2] *Reducing emissions from transport*. [Online]
Available at: ec.europa.eu/clima/policies/transport [Accessed 20/05/2014]

[3] Sullivan, R.A., "Automotive Carbon Fiber: Opportunities and Challenges," JOM, pp. 77-79, November, 2006.

[4] Lin, J., Jin, Y., Zhang, Z., Cui, X., 2014. *Strength analysis of the Carbon-Fiber Reinforced Polymer Impeller Based on Fluid Solid Coupling Method*. In: Mathematical problems in Engineering. Hindawi Publishing Corporation. Vol. 2014. Article ID 803261.

[5] W.V. Chaves, E., 2013. *Notes on Continuum Mechanics.* Barcelona, Spain: International Center for Numerical Methods in Engineering (CIMNE).

[6] McGinty, B., 2014. *Finite Deformation Continuum Mechanics with emphasis on metals & incompressible materials*. [Online]
Available at: http://www.continuummechanics.org [Accessed 19/03/2014]

[7] Ferrer, M., 2014. *Continuum mechanics* (ETSEIB-UPC). (in Catalan) [Online]
Available at: http://mmc.etseib.upc.edu [Accessed 29/03/2014]

[8] Gay, D. & Hoa, S. V., 2007. Composite Materials, Interest, and Properties. In: *Composite Materials: Design and Applications,* 2nd ed. Boca Raton, FL: Taylor&Francis Group.

[9] Gay, D. & Hoa, S. V., 2007. Ply Properties. In: *Composite Materials: Design and Applications,* 2nd ed. Boca Raton, FL: Taylor&Francis Group.

[10] Hull, D. & Clyne, T.W., 1996. *An introduction to Composite Materials* (Cambridge solid state science series), 2nd ed. Cambridge, United Kingdom: Cambridge University Press.

[11] Agarwal, B. D. & Broutman, L. J., 1990. *Analysis and performance of fiber composites*, 2nd ed. New York: John Wiley & Sons, Inc.

[12] Santin, J.J., Onder, C.H., Bernard, J., Isler, D., Kobler, P., Kolb, F., Weidmann, N., & Guzzella, L., 2007. Wheels. In: *The World's Most Fuel Efficient Vehicle. Design and Development of PAC car II.* Zürich: vdf Hochschulverlag AG an der ETH Zürich.

[13] Stoltze, J. S., Nielsen, M. B., Pedersen, S. V., Petersen, N. H., Peters, R. A. W., & Garroguerricaechevarria, I. A., 2013. *Optimisation of Rims for Shell Eco-Marathon Vehicle to Improve Fuel Efficiency*. In: The 1st student symposium on mechanical and manufacturing engineering, 21st of June, 2013. Aalborg University. Aalborg, Denmark.

[14] Prat Bartés, A., Tort-Martorell Llabrés, X., Grima Cintas, P. & Pozueta Fernández, L., 1997. *Statistical methods. Control and Quality Improvement.(in Spanish)* Barcelona, Spain: Edicions UPC.

[15] Box, G., Behnken, D., 1960. *Some new three level designs for the study of quantitative variables*, Technometrics, Volume 2, pp. 455–475.

[16] Gay, D. & Hoa, S. V., 2007. Conception and Design. In: *Composite Materials: Design and Applications,* 2nd ed. Boca Raton, FL: Taylor&Francis Group.

[17] Wünsche, B. 1999. *The visualization of 3d stress and strain tensor fields.* Department of Computer Sciencem, Univeristy of Auckland. Auckland, New Zealand.

[18] The stress tensor. [Online]
Available at: http://www.efunda.com/formulae/solid_mechanics [Accessed 19/03/2014]

[19] Tanaka, Y. & Bauer, R. S., 1988. Curing Reactions. In: *Epoxy Resins. Chemistry and Technology,* 2nd ed, revised and expanded. New York, NY: Marcel Dekker, Inc.

[20] Hedad, D.K., 1988. Physical and Chemical Characterization of Epoxy Resins In: *Epoxy Resins. Chemistry and Technology,* 2nd ed, revised and expanded. New York, NY: Marcel Dekker, Inc.

[21] Delmonte, J., Hoggatt, J.T., May, C. A., 1988. Fiber-Reinforced Epoxy Composites. In: *Epoxy Resins. Chemistry and Technology,* 2nd ed, revised and expanded. New York, NY: Marcel Dekker, Inc.

[22] Lew, P., 2014. *Understanding Wheel Dynamics: Carbon Fiber Variability*. [Online] Available at: http://www.reynoldscycling.com/reynolds/news/Understanding-Wheel-Dynamics:-Carbon-Fiber-Variability [Accessed 24/04/2014]

[23] *Brent Strong, A., 2008. Fundamentals of Composites Manufacturing. Materials, methods, and applications*. 2nd edition. Dearborn, Michigan: Society of Manufacturing Engineers. pp. 322-323.

[24] ANSYS® Help

[25] Hill, R., 1948. *A Theory of the Yielding and Plastic Flow of Anisotropic Metals.* In: Proceedings of the Royal Society of London, Series A, 193, pp. 281-297.

[26] Von Mises, R., "*Mechanics of Solids in Plastic Deformation state,"* (in German) Nachr. Ges. Wiss. Gottingen, 1913, pp. 582.

[27] Tsai, S. W. & Wu, E. M., 1971. *A general theory of strength for anisotropic materials,"* Journal of Composite Materials. Vol. 5, 1971, pp. 58–80.

[28] Tsai, S. W., 1968. *Strength theories of filamentary structures.* In: Fundamental Aspects of Fibre Reinforced Plastic Composites, Conference Proceedings, R. T. Schwartz and H. S. Schwartz (Editors), Dayton, Ohio, 24-26 May 1966, Wiley Interscience, New York. pp. 3-11.

[29] Turner, M.J., Clough, R.W., Martin, H.C. and Topp, L.J., *"Stiffness and deflection analysis of complex structures,"* J. Aero. Sci., 23, 1956, pp. 805–823.

[30] Moaveni, S., 2008. *Finite Element Analysis. Theory and application with ANSYS,* 3rd ed. Upper Saddle River, NJ: Pearson International Edition.

[31] Mindlin, R. D., 1951. *Influence of rotatory inertia and shear on flexural motions of isotropic, elastic plates*. In: ASME Journal of Applied Mechanics, Vol. 18 pp. 31–38.

[32] Reissner, E., 1945. *The effect of transverse shear deformation on the bending of elastic plates*. In: ASME Journal of Applied Mechanics, Vol. 12, pp. A68-77.

[33] Shell Eco-marathon®, 2014. Chapter 1. In: *Shell Eco-marathon Official Rules 2014.*[Online] Available at: http://www.shell.com/global/environment-society/ecomarathon/for-participants/general-information/rules.html [Accessed 15/04/2014]

[34] Knupe, J. & Farmer, D., 2014. *Aerodynamics of High Performance Race Bicycle Wheels.* [Online] Available at: http://www.wing-light.de/CFD/CFD [Accessed 04/04/2014]

[35] Gay, D. & Hoa, S. V., 2007. Joining and Assembly. In: *Composite Materials: Design and Applications,* 2nd ed. Boca Raton, FL: Taylor&Francis Group.

[36] Hollaway, L.C., 1994. Manufacturing processes. In: *Handbook of Polymer Composites For Engineers*. Cambridge, England: Woodhead Publishing Ltd.

8 Appendixes

A. Generalized Hooke's law

The generalized Hooke's law relates the stress and strain tensors. The matrix [C] contains all the material constants for relating the stresses with the strains. For isotropic materials just two constants are needed and for orthotropic nine, a particular case of anisotropic material where 21 constants are needed.

- Isotropic materials:

Two independent constants: $c_1 = \frac{1}{E}$, $c_2 = \frac{-\nu}{E}$

$$\begin{Bmatrix} \varepsilon_{11} \\ \varepsilon_{22} \\ \varepsilon_{33} \\ \varepsilon_{12} \\ \varepsilon_{13} \\ \varepsilon_{23} \end{Bmatrix} = \begin{bmatrix} c_1 & c_2 & c_2 & 0 & 0 & 0 \\ c_2 & c_1 & c_2 & 0 & 0 & 0 \\ c_2 & c_2 & c_1 & 0 & 0 & 0 \\ 0 & 0 & 0 & c_1 - c_2 & 0 & 0 \\ 0 & 0 & 0 & 0 & c_1 - c_2 & 0 \\ 0 & 0 & 0 & 0 & 0 & c_1 - c_2 \end{bmatrix} \begin{Bmatrix} \sigma_{11} \\ \sigma_{22} \\ \sigma_{33} \\ \sigma_{12} \\ \sigma_{13} \\ \sigma_{23} \end{Bmatrix}$$

- Orthotropic materials:

Nine independent constants:

$$c_1 = \frac{1}{E_1},\ c_2 = \frac{1}{E_2},\ c_3 = \frac{1}{E_3},\ c_4 = \frac{-\nu_{12}}{E_2},\ c_5 = \frac{-\nu_{13}}{E_3},\ c_6 = \frac{-\nu_{23}}{E_3},\ c_7 = \frac{1}{2G_{12}},\ c_8 = \frac{1}{2G_{13}},\ c_9 = \frac{1}{2G_{23}}$$

$$\begin{Bmatrix} \varepsilon_{11} \\ \varepsilon_{22} \\ \varepsilon_{33} \\ \varepsilon_{12} \\ \varepsilon_{13} \\ \varepsilon_{23} \end{Bmatrix} = \begin{bmatrix} c_1 & c_4 & c_5 & 0 & 0 & 0 \\ c_4 & c_2 & c_6 & 0 & 0 & 0 \\ c_5 & c_6 & c_3 & 0 & 0 & 0 \\ 0 & 0 & 0 & c_7 & 0 & 0 \\ 0 & 0 & 0 & 0 & c_8 & 0 \\ 0 & 0 & 0 & 0 & 0 & c_9 \end{bmatrix} \begin{Bmatrix} \sigma_{11} \\ \sigma_{22} \\ \sigma_{33} \\ \sigma_{12} \\ \sigma_{13} \\ \sigma_{23} \end{Bmatrix}$$

B. Optimum Composition of a Laminate

This appendix presents the tables used for finding the optimum orientation of the fibres. If one known the stress proportions given a reference orientation, these table allow to find the percentage of fibres that should be placed at the four main orientations (0°, 90°, 45° and -45°).

Table 12. Optimum Composition of a Carbon/Epoxy Laminate. ($+N_x$ / $+N_y$) [12]

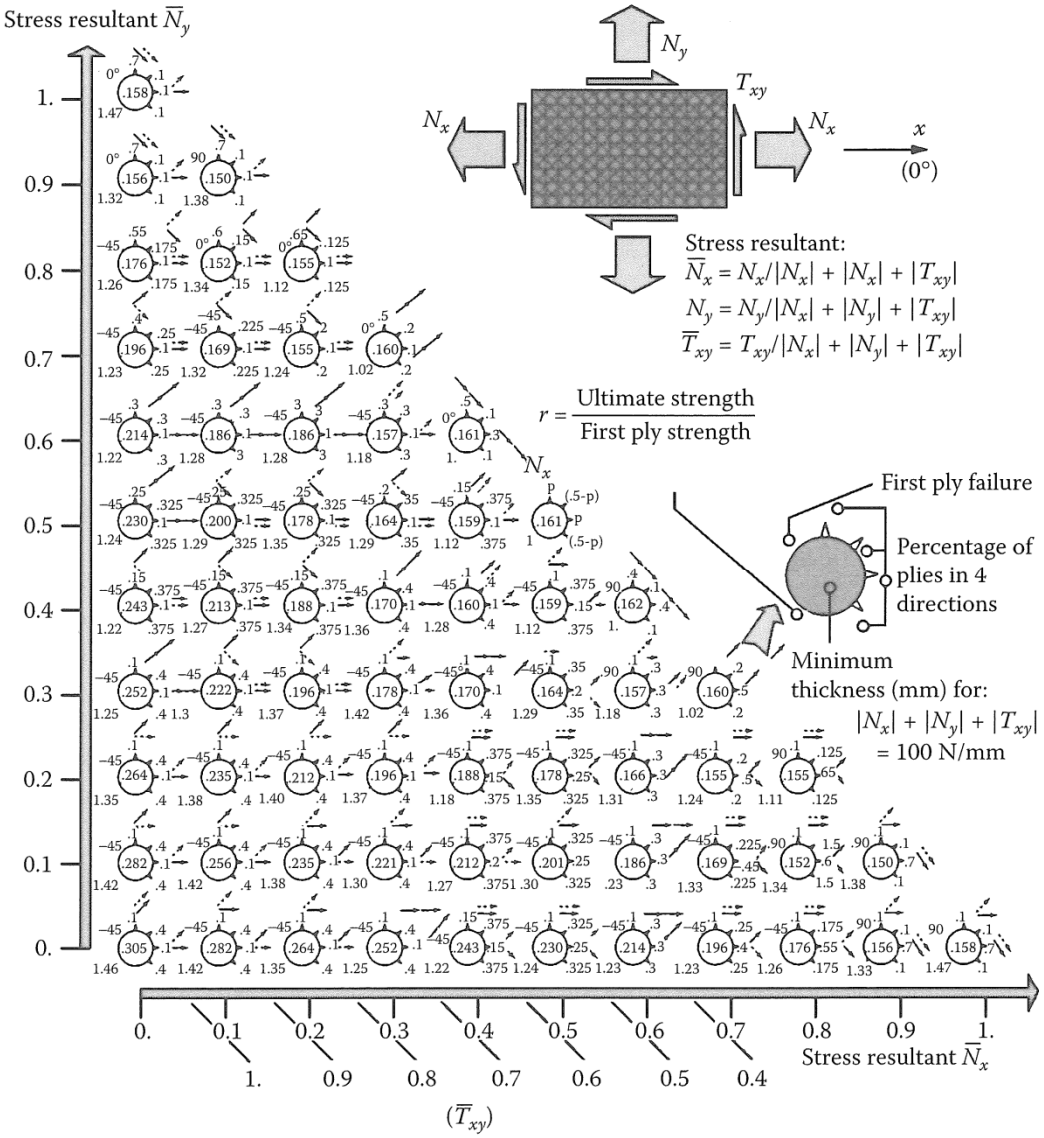

Table 13. Optimum Composition of a Carbon/Fibre Laminate. ($-N_x/+N_y$). [12]

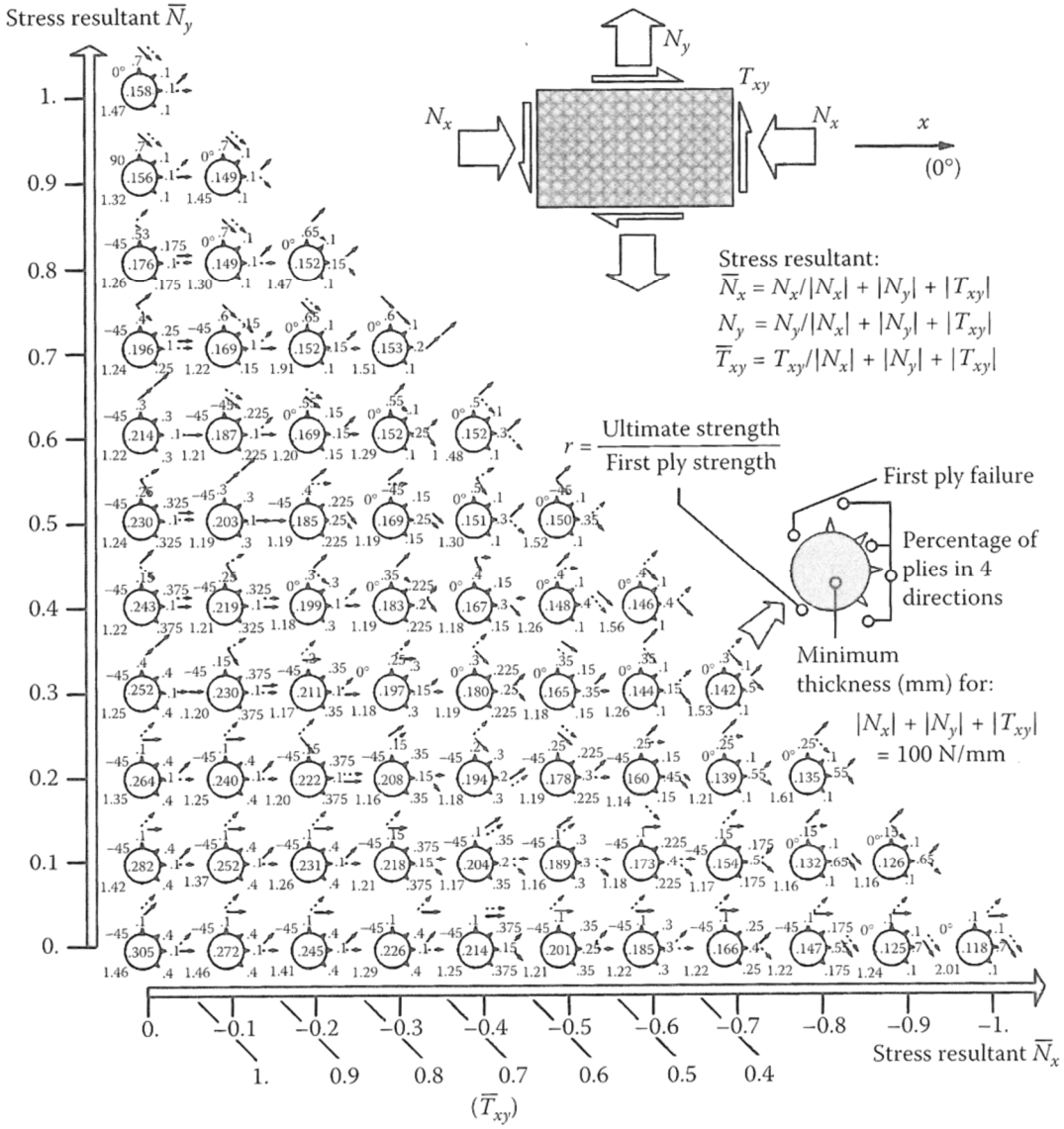

C. Polar representation of the elastic properties

The following figures illustrates the elastic properties of different layers but in a polar diagram. The polar diagrams allow us to visualize how the properties changes with variation of the testing angle. Comparing both figures one can appreciate the difference between unidirectional and woven fabrics, the first more anisotropic. For the woven fabric, the properties on the longitudinal and transverse orientations (*E*1 and *E*2) are the same then the two properties are superimposed on the figure.

The *E*1 can be understood as *E* (modulus of elasticity) on the fibre direction (or zero degree orientation) and the *E*2 as transverse to the fibre's direction (90 degrees orientation). *G*12 is the shear modulus on plane. The radius represents the values of the modulus, where the magnitudes are MPa.

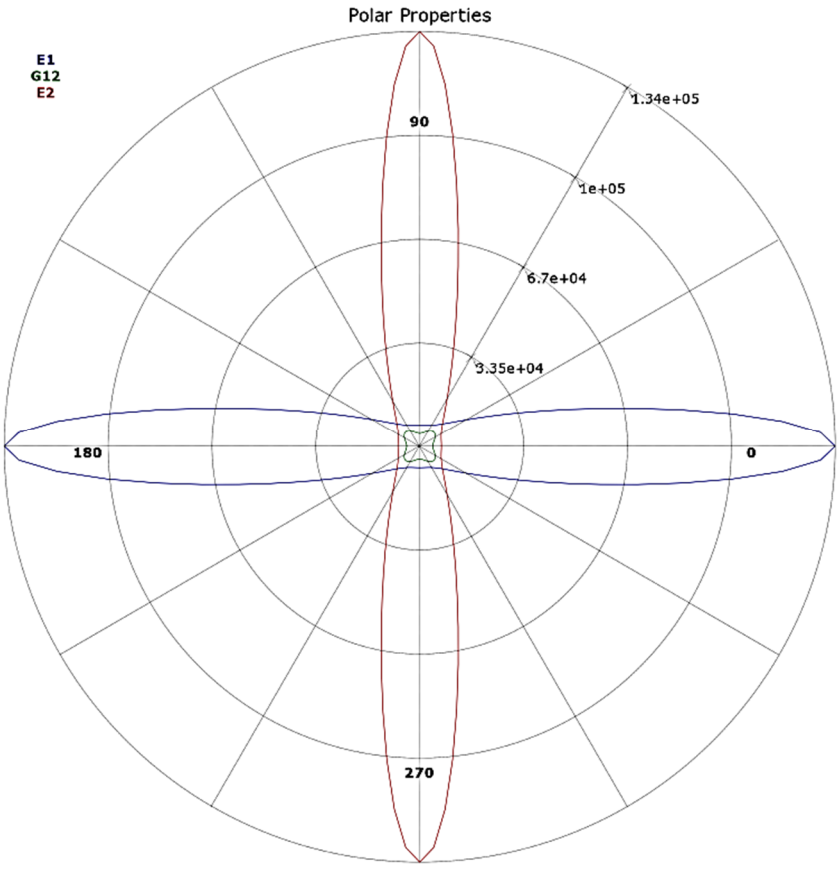

Figure 46. Polar representation of the elastic properties. Unidirectional ply. [MPa]

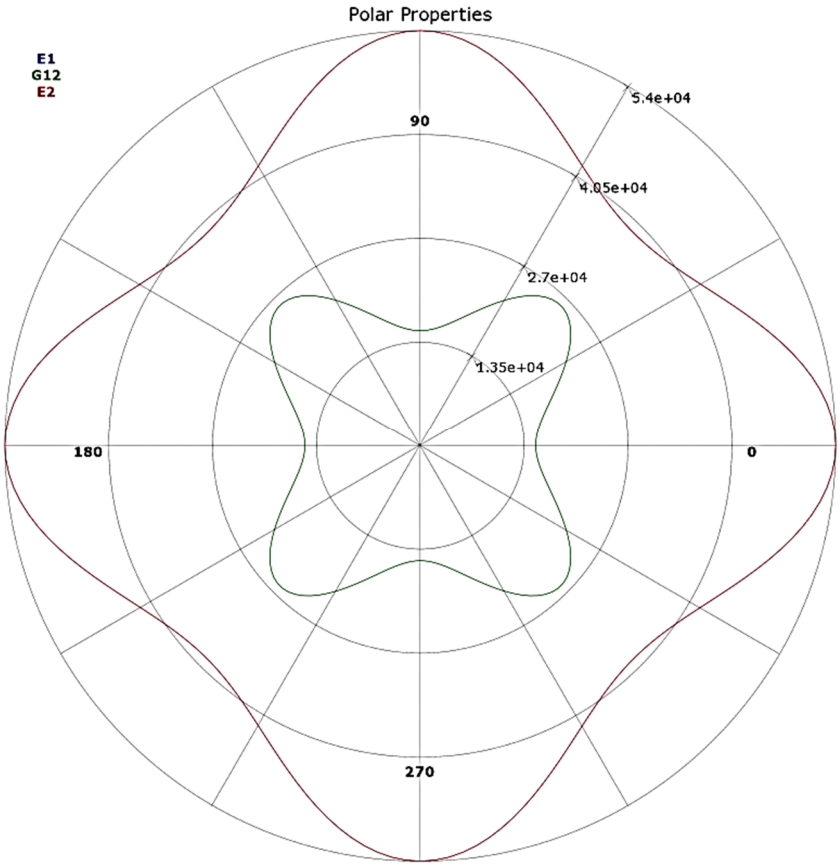

Figure 47. Polar representation of the elastic properties. Plain weave woven fabric. [MPa]

D. Tsai-Hill criterion

Source: [24].

In quadratic criteria all the stress or strain components are combined into one expression. Many commonly used criteria for fibre-reinforced composites belong to a subset of fully interactive criteria called quadratic criteria. The general form of quadratic criteria can be expressed as a second-degree polynomial.

$$f = F_{11}\sigma_1^2 + F_{22}\sigma_2^2 + F_{33}\sigma_3^3 + F_{44}\tau_{23}^2 + F_{55}\tau_{13}^2 + F_{66}\tau_{12}^2 + 2F_{12}\sigma_1\sigma_2 + 2F_{23}\sigma_2\sigma_3 + 2F_{13}\sigma_1\sigma_3 + F_1\sigma_1 + F_2\sigma_2 + F_3\sigma_3$$

In plane stress-state (s3=0), the polynomial reduces to the simpler form

$$f = F_{11}\sigma_1^2 + F_{22}\sigma_2^2 + F_{66}\tau_{12}^2 + 2F_{12}\sigma_1\sigma_2 + F_1\sigma_1 + F_2\sigma_2$$

In the Tsai-Hill criterion, either tensile or compressive strengths are used for determining the coefficients F depending on the loading condition. The coefficients are

$$F_{11}=\frac{1}{X^2} \quad F_1=0 \quad F_{12}=-\frac{1}{2X^2}$$
$$F_{22}=\frac{1}{Y^2} \quad F_2=0$$
$$F_{44}=\frac{1}{Q^2} \quad F_{55}=\frac{1}{R^2} \quad F_{66}=\frac{1}{S^2}$$

where the values of X and Y are

$$\sigma_1 \geq 0 \Rightarrow X=X_t \quad ;\sigma_1<0 \quad \Rightarrow X=X_c$$
$$\sigma_2 \geq 0 \Rightarrow Y=Y_t \quad ;\sigma_2<0 \quad \Rightarrow Y=Y_c$$

Hence, the Tsai-Hill failure criterion function can be written in the form

$$f=\left(\frac{\sigma_1}{X}\right)^2+\left(\frac{\sigma_2}{Y}\right)^2+\left(\frac{\tau_{23}}{Q}\right)^2+\left(\frac{\tau_{13}}{R}\right)^2+\left(\frac{\tau_{12}}{S}\right)^2-\frac{\sigma_1\sigma_2}{X^2}$$

For the full 3D case another formulation can be used as:

$$(G+H)\sigma_1^2+(F+H)\sigma_2^2+(F+G)\sigma_3-2H\sigma_1\sigma_2-2G\sigma_1\sigma_3-2F\sigma_2\sigma_3 \ldots$$
$$+2L\tau_{23}^2+2M\tau_{13}^2+2N\tau_{12}^2=1$$

where

$$F=\frac{1}{2}\left(-\frac{1}{X^2}+\frac{1}{Y^2}+\frac{1}{Z^2}\right)$$
$$G=\frac{1}{2}\left(\frac{1}{X^2}-\frac{1}{Y^2}+\frac{1}{Z^2}\right)$$
$$H=\frac{1}{2}\left(\frac{1}{X^2}+\frac{1}{Y^2}-\frac{1}{Z^2}\right)$$